Designing a Novel 3D *In-Vitro* Model of Mechanical Stress on Dystrophic Aortic Valve Calcification

A Major Qualifying Project Report:
Submitted to the faculty of

WORCESTER POLYTECHNIC INSTITUTE

In partial fulfillment of the requirements for the
Degree of Bachelor of Science

Submitted by:

Beck Arruda

Marina Christakos

Karla Cuellar

Alyssa Sousa

Date: May 6, 2021

Table of Contents

List of Figures

List of Tables

Abstract

Calcific aortic valve disease (CAVD) is the most common valvular heart disease in the world. Understanding more about the mechanism of CAVD will improve prevention and treatment approaches. The project aimed to design a 3D *in-vitro* model to investigate the effects of mechanical stress on dystrophic VIC calcification. The design consisted of spheroids embedded in various hydrogels (collagen, fibrin, and GelMA+HAMA), resulting in viable constructs with a range of properties. The constructs were stretched at 10% strain with a cell stimulator (CellSCale MCFX). Further testing should be completed to characterize the interactions between the spheroids and hydrogels and to validate calcification.

Chapter 1: Introduction

Calcific aortic valve disease (CAVD) is the most common valvular heart disease (Yutzey et al, 2014). By 2030, the disease is expected to affect 4.5 million people - a 2 million person increase since 2000 (Lerman et al, 2015). Over 25% of people over the age of 65 show signs of the disease, which leads to a 50% increase in future heart diseases, and a risk that within 5 years, patients have an 80% chance of either heart failure, valve replacement, or death (Yutzey et al, 2014).

CAVD occurs when calcium deposits form on the aortic valve and cause the opening of the valve to narrow (Yutzey et al, 2014). CAVD has several stages, ranging from a mild form of calcification to a life-threatening progression. The mild form of CAVD is called aortic sclerosis, which mildly thickens the valve but does not obstruct blood flow. CAVD can eventually lead to a more serious condition, called aortic valve stenosis, which impairs leaflet motion and involves extreme calcification (Lerman et al, 2015).

During aortic valve calcification, the normal valve ECM can become disturbed when subjected to either biochemical or mechanical stress. When such a disruption occurs, there is a continuous fibrosis and thickening of the leaflets of the aortic valve which result in calcification as well as inflammation, neovascularization, and ectopic tissue. The calcified areas of tissue are most commonly extended from the fibrosa layer of the heart valve to the aortic region of the heart valves, the calcified nodules can put the valve's function and its integrity at risk (Leopold, 2012).

In order to better understand calcification within valvular interstitial cells (VICs), researchers have worked to create several types of cell culture models. These can be separated into two categories: *in-vivo*, which utilizes animals, and *in-vitro* 3D cell culture, which has the opportunity to use animal or human primary cells or cell lines.

Biological calcification *in-vivo* is a complex series of events that must be heavily regulated in order to occur at the right time, location, stage, and maturity (Zuppinger, 2019). The most commonly used animal models to display *in-vivo* calcification are rabbits, mice, and pigs. On an anatomical level, the pig and rabbit have similar anatomy because they have a trilayer valve tissue, while the mouse does not (Sider et al, 2011). Even with the similarities and benefits, no model is perfect and all three require dietary or genetic changes to exhibit CAVD (Bowler & Merryman,2015). While calcification occurs in all of the listed animal models, it may not be representative of human disease. These models are expensive and extremely complex relative to 3D cell culture, as they require long-term housing and care in addition to experienced personnel (Zuppinger, 2019).

In-vitro models of calcification are more controlled than the *in-vivo* discussed above. These models can be separated into two-dimensional and three-dimensional. Two-dimensional models are much more common, whereas 3D models began developing more recently. Calcification mechanisms are more straightforward to study in 2D systems of VICs, giving importance to 2D models and understanding calcification from the *in-vitro* standpoint. These models are also more inexpensive, well established in terms of research, and easier for cell observation (Duval et al, 2017). While 2D systems have some benefits, it can be considered misleading when they are used to model the physiological responses of the body (Zuppinger,

2019). The most accurate cells that can be used to model calcification are human primary VIC cells, however they are difficult to access (Bowler & Merryman, 2015). Culture of cells in a 2D environment often results in the loss of cellular differentiation or loss of cell function (Mabry, 2016).

In vitro 3D systems of VICs would be beneficial in order to study CAVD mechanisms in an environment with high levels of control (Mabry et al, 2016). Three-dimensional cell culture has become extremely important because it allows for some of the limitations of two-dimensional cell culture to be overcome by providing a more accurate representation of the *in vivo* microenvironment of the system (Roosens et al, 2017). Cells grown in a 3D model have proven to be more physiologically relevant and showed improvements in several studies of biological mechanisms like: cell number monitoring, viability, morphology, proliferation, differentiation, response to stimuli, general cell function, and *in-vivo* relevance (Antoni et al, 2015). Aside from the benefits, 3D models are much more expensive, complex, and unfamiliar to researchers. Current 3D models also only show osteogenic calcification, the less prevalent type of calcification, which brings the team to the project's goal.

The goal of this project is to design a 3D *in-vitro* model to study the mechanism of valvular interstitial cells (VIC) dystrophic calcification under mechanically dynamic conditions. The following criteria must be considered in the design process: cost, ease of use, ability to rapidly calcify, mechanically stress cells, model aortic valve biochemistry, model aortic valve ECM, and model dystrophic calcification. The design process utilized to accomplish the task followed the typical engineering design process. The team interviewed the client in order to determine what needed to be accomplished. The client also provided important details regarding selecting objectives and potential functions for the design. The objectives were ranked, a function-means table was created, and multiple designs were created. Feasibility studies focusing on operational goals, economic goals, technical goals, and scheduling of the project were performed on different design elements to optimize the final design and prototype.

Chapter 2: Literature Review

In this section, current theories of how CAVD progresses and what techniques are currently used to model it *in-vitro*, including animal and three-dimensional cell culture models, are discussed.

2.1 Calcific Aortic Valve Disease

Calcific aortic valve disease (CAVD) is the most common valvular heart disease (Yutzey et al., 2014). By 2030, the disease is expected to affect 4.5 million people - a 2 million person increase since 2000 (Lerman et al., 2015). Over 25% of people over the age of 65 show signs of the disease, which leads to a 50% increase in future heart diseases, and a risk that within 5 years, patients have an 80% chance of either heart failure, valve replacement, or death (Yutzey et al., 2014).

The aortic valve consists of three collagen leaflets attached to a fibrous ring at the outlet of the left ventricle (Figure 1). These leaflets are normally thinner than 1 mm and are composed of extracellular matrix (ECM) separated into three layers: lamina fibrosa, lamina spongiosa, and lamina ventricularis (Rutkovskiy et al., 2017). The lamina fibrosa is rich in type I and III collagen fibers, which allow it to withstand high pressure loads. The lamina spongiosa proteoglycans which offer compression resistance and lubrication. The lamina ventricularis is composed of elastic fibers that allow preload for stretch and recoil. These three layers are extremely populated with valve interstitial cells (VICs) and covered with valve endothelial cells (VECs) (Zhang et al., 2015).

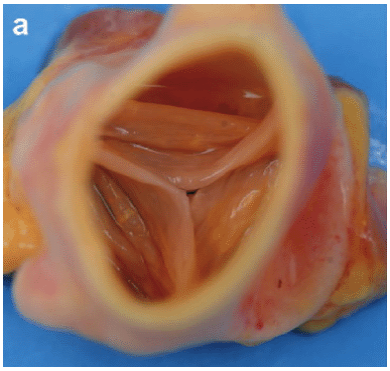

Figure 1: Aortic valve leaflet anatomy [Reproduced with copyright approval, Weymann, 2012]

CAVD has several stages, ranging from a mild form of calcification to a life-threatening progression, as shown in Figure 2. The mild form of CAVD is called aortic sclerosis, which mildly thickens the valve but does not obstruct blood flow. CAVD can eventually lead to a more serious condition, called aortic valve stenosis, which impairs leaflet motion and involves extreme calcification (Lerman et al., 2015).

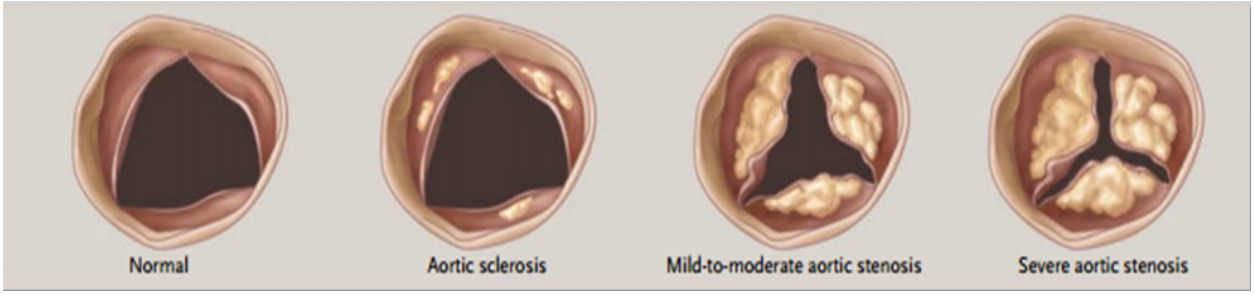

Figure 2: The progression of CAVD [Reproduced with copyright approval, Otto, 2008]

The only current treatment method is heart surgery to implement a prosthetic valve. This will either be a mechanical valve that requires life-long anticoagulation treatment (Figure 3), or a bioprosthetic valve (Figure 4) which will degenerate and need to be replaced within 10-15 years (Rutkovskiy et al., 2017). Though there are currently methods, they are considered to be temporary fixes rather than a cure. Understanding more about CAVD and calcification can likely offer more permanent treatment opportunities.

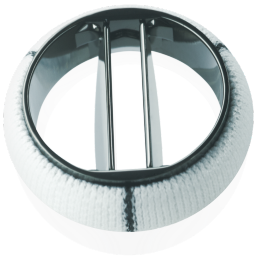

Figure 3: Mechanical valve [Reproduced with copyright approval, Vdkerkhof, 2011]

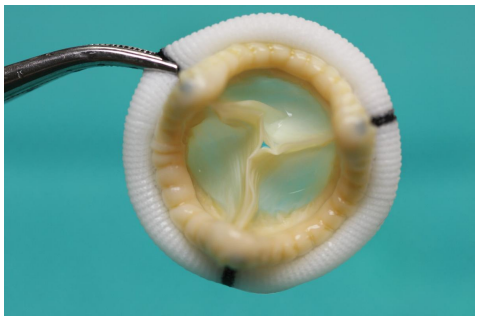

Figure 4: Bioprosthetic valve [Reproduced with copyright approval, Vyavahare, 2018]

2.1.1 Risk Factors for CAVD

There are a variety of factors correlated with CAVD, including older age, male sex, smoking, hypertension, high LDL cholesterol levels, and being overweight (Chen et al., 2019). Many of these are applicable to other cardiometabolic diseases and are therefore called cardiometabolic risk factors. While CAVD used to be considered an unregulated, degenerative disease, it is now considered to be a more active process involving multiple cellular and molecular mechanisms (Im Cho et al., 2018).

A significant factor influencing the cellular mechanisms in the heart valves is blood pressure and mechanical stress. Cells experience a variety of stresses in the body, namely compressive, tensile, and shear stress (Shah et al., 2014). VICs undergo a significant amount of tensile stress during diastole while the valve is closed, and the leaflets are stretched about 10% (Balachandran et al., 2014). However, with increasing blood pressure, there is an increase in stretch. There is roughly a 5% increase in stretch given a 40mmHg increase in pressure (Balachandran et al., 2011). The risk of CAVD increases with hypertension; 60% of CAVD patients have hypertensive blood pressure (Chen et al., 2019).

2.1.2 Mechanical Properties of Calcified Heart Valves

When considering a model which allows one to observe calcification *in-vivo,* the system needs to be able to stimulate the natural ECM of the valve in the environment of the *fibrosa* valve layer, where calcification is mainly observed (Hjortnaes et al., 2016). There currently are not many effective systems that effectively model calcification. In 2D systems, a problem occurs because the environment does not accurately portray that of the native heart valve. When VIC cells are isolated from tissue and plated on 2D culture dishes, a wound-healing response begins. It differentiates from quiescent fibroblasts to activate myofibroblasts, which creates a heterogeneous population. This leads to the formation of multicellular aggregates and calcified nodule structures (Benton et al., 2009). A successful 3D system needs to avoid these errors to better mimic the conditions of a human aortic valve. This will be done by creating a system that has similar mechanical properties to the *fibrosa* valve layer before and after calcification. The modulus of a healthy aortic valve is 7 kPA, and a calcified valve is 32 kPa (Wang et al., 2012).

Normal valve tissue matrix is considered a loose and hydrated network containing glycoproteins, which can cause the matrix to become dense. However, during calcification the ECM of VICs contains much more collagen and fibronectin than normal vascular cells, causing VICs to mineralize and have a more adhesive and stiff substrate (Lim et al., 2016). Fibronectin is a glycoprotein that binds to receptor proteins, integrin, as well as other ECM proteins (Bierbaum et al., 2017). Integrin connections between cytoskeletal fibers and ECM proteins have various effects on cell behavior and shape as well as differentiation. As calcification progresses, the intima thickens with an increase in other matrix proteins as well (thrombospondin, tenascin, osteopontin, osteocalcin, dentin matrix acidic phosphoprotein 1) (Hsu et al., 2016).

2.1.3 The Role of VICs in Calcification

Calcification is the process in which calcium accumulates in body tissue, blood vessels or organs resulting in the area affected to harden. During aortic valve calcification, the normal valve ECM can become disturbed when subjected to either biochemical or mechanical stress. When such a disruption occurs, there is a continuous fibrosis and thickening of the leaflets of the aortic valve which result in calcification as well as inflammation, neovascularization, and ectopic tissue. The calcified areas of tissue are most commonly extended from the fibrosa layer of the heart valve to the aortic region of the heart valves, the calcified nodules can put the valve's function and its integrity at risk (Leopold, 2012).

Passive calcification can occur in the body through the slow deposition of circulating calcium in the bloodstream, but CAVD is recognized as being a result of active cellular processes (Im Cho et al., 2018). There are two primary forms of active calcification associated with CAVD: dystrophic and osteogenic (Bowler & Merryman, 2015). Osteogenic calcification occurs as a result of VICs adopting an osteoblast-like phenotype. These osteoblast-like cells produce an osteoid matrix. In a study of human valve explants, osteogenic calcification was found in only 13%, while dystrophic calcification was found in 83% (Mohler, 2001). Dystrophic is believed to occur when the normally quiescent VICs are activated and adopt a myofibroblast-like phenotype. These calcify via an apoptotic mechanism. Further evidence for a mechanically driven dystrophic pathway is the prevalence of CAVD in bicuspid valves, which undergo more stress than the normal tricuspid valves (Balachandran et al., 2011).

2. 2 Cell-Mediated Calcification

Biological calcification *in-vivo* is a complex series of events that must be heavily regulated in order to occur at the right time, location, stage, and maturity. This responsibility is primarily given to cells with osteoblastic lineage (Gilbert, 2000). VICs activated by the inflammatory process are designated myofibroblasts (Otto et al., 1994). The inflammation will promote angiogenesis which allows for increased delivery of oxygen and nutrients to the injured tissue. The activation of the VICs results in the production matrix metalloproteinases, which are proteins that are involved in tissue remodelling. During this process, activated VICs may also differentiate into osteoblasts (Lerman et al., 2015).

While it is possible to analyze cellular activity through immunological techniques, research shows that directly influencing biological calcification by osteoblastic cells is best obtained in an *in-vitro* environment, where variables can be systematically evaluated. Therefore, the development of tissue and cell culture model systems is extremely important (Gilbert, 2000).

2.2.1 Human Pathology

CAVD has specific pathological features. Calcification begins near the edges of the valve, near to where it attaches. However, the calcific nodules can extend all throughout the cusps, especially with the advancement of the disease (Rajamannan, et.al., 2011). The morphological state of calcification can range from sclerosis, which is the pathological hardening of the cardiac tissue, to stenosis, the almost total narrowing or constriction of a vessel. Lipids have also proven to signal valvular calcification. Histopathologic studies have demonstrated plaquelike lesions on the valve leaflets that extend to the fibrosa layer. These lesions are hypothesized to be initiated by endothelial disruption due to mechanical stress (Freeman et al., 2005). Accumulation of lipids and presence of inflammatory cells can lead to the formation of extracellular matrices that could potentially remodel and calcify.

CAVD has been studied extensively in hopes of identifying key epidemiological factors that contribute to it (Yutzey, et.al., 2014). The cause of this disease has not been found yet, but certain factors that contribute to its pathogenesis have been identified. One of the major limitations of what is known about this disease is that it is extremely difficult to identify the risk before the symptoms appear. Further studies are required in order to provide a better understanding of the disease and the population groups it targets.

2.2.2 In Vivo Models of Calcification

In order to understand how calcification functions in humans, there first needs to be a comprehensive model that allows researchers to observe CAVD *in-vivo*, considering the complex mechanical, electrical, and biochemical forces which act upon the valve (Zuppinger, 2019). The most commonly used animal models are rabbits, mice, and pigs. On an anatomical level, the pig and rabbit have similar anatomy because they have a trilayer valve tissue, while the mouse does not (Sider et al., 2011). Even with the similarities and benefits, no model is perfect and all three require dietary or genetic changes to exhibit CAVD (Bowler & Merryman, 2015).

The mouse needs a high cholesterol diet and develops mild hypercholesterolemia over time, but there is o not enough evidence to see if it passes through the same mechanism as humans, since they do not have similar leaflet anatomy (Sider et al., 2011). The rabbit has significant differences in lipid metabolism from humans which can cause cholesterol storage syndrome. In order to induce CAVD and in some cases

they use vitamin D treatment which will accelerate calcification. Pigs can spontaneously develop atherosclerotic lesions, which is a precursor to CAVD. In order to accelerate the process for research, there must be a diet induced hypercholesterolemia, which would cause lipoprotein levels to rise (Bowler & Merryman, 2015). Other animals that are commonly used are cows, dogs, sheep, and rats, but regardless of which animal is used, either genetic or dietary changes are needed to make the model better mimic the functions of human calcification.

While calcification is possible to occur in all the animal models discussed, it is very difficult to achieve. However, animal models allow the study of signaling pathways under controlled conditions. Ultimately, animal models are expensive and extremely complex relative to 3D cell culture, as they require long-term housing and care in addition to experienced personnel (Zuppinger, 2019). In order to truly understand the relevance of animal models to human calcification, a better understanding of human CAVD pathogenesis is required.

2.2.3 Two-dimensional Models

Current 2D models result in cells appearing in a flat and spread out form. This structure allows for easy validation of cells' function and pathology (Soares et al., 2012). The physiological responses of the body result in the cells experiencing stimuli such as biochemical, mechanical, and electrical, which shape how they behave, which can be controlled and studied in 2D.

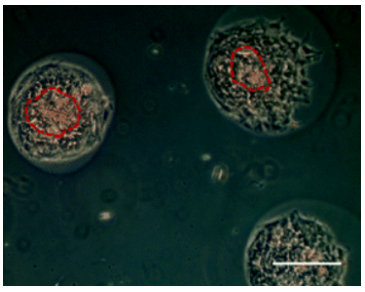

Figure 5: Dystrophic 2D Model [Reproduced with copyright approval, Circa et al., 2017]

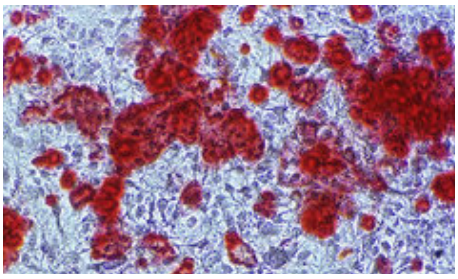

Figure 6: Osteogenic 2D Model [Reproduced with copyright approval, Zabirnyk et al., 2019]

Calcification mechanisms are more straightforward to study in 2D systems of VICs, giving importance to 2D models and understanding calcification from the *in-vitro* standpoint. One of the main problems of working with VIC is the control of their activated/quiescent state. Culture of cells in a 2D environment often results in the loss of cellular differentiation or loss of cell function. It is known that when VIC are cultured in 2D, on cell culture plastics or seeded on synthetic/biological scaffolds to provide a substrate allowing cell migration and repopulation of the scaffold, they become activated (aVIC). Finding the optimal culture conditions in which VIC could preserve or regain their native, fibroblast-like quiescent phenotype while promoting VIC-mediated ECM production, could be promising for the development of a tissue engineered living valve substitute. 2D cell culture systems mimic more closely the actual *in-vivo* micro-environment. Moreover, they allow better cell-to-cell and cell-to-matrix interactions than other systems, which are important for cell differentiation, proliferation and cellular functions, and which also stimulate cells to produce ECM components and to organize into microtissue-like structures *in-vitro* (Mabry, 2016).

2.2.4 Three-dimensional Models

A relevant current 3D model is *in-vitro* 3D cell culture, which has the opportunity to use animal or human primary cells or cell lines. The benefit of 3D *in-vitro* models is that they have greater physiological cell morphology and signaling than that of 2D cell culture. Additionally, 3D models allow for quick manipulations while experimenting and hypothesis testing as well as allow for enhanced imaging by microscopy than in animals.

There are currently limitations with 3D VIC models as they do not have the aggregation that is observed in CAVD, and most of these 3D models lack dynamic stretching as well. 3D VIC models also have inconsistent ability to emulate tissue conditions *in-vivo* well and for extended periods of time often only being able to imitate short-term conditions. Structurally, 3D models lack vasculature and normal transport of small molecules, host immune response and other cell-cell interactions.

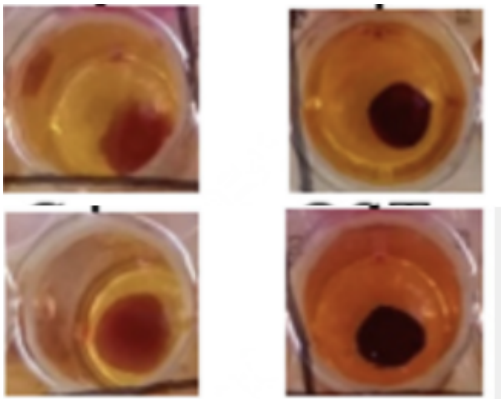

Figure 7: 3D Osteogenic Model [Reproduced with copyright approval, Vadana, et al., 2020]

There are currently a few types of *in-vitro* 3D models, though none of these are used to model CAVD. One type commonly used is the harvesting of tissues *in-vivo*, using intact tissue pieces or embryonic organs that are microscopic in size, either is then explanted and cultured *in-vitro*, and are able to maintain their structure while *in-vitro*. This particular type of 3D model is beneficial for cultures that are short lived (Yamada & Cukierman, 2007).

Table 1: Differences between 2D and 3D Models (From Yamada & Cukierman, 2007)

Biological function	2D vs. 3D	Regulatory Mechanisms
Cell Shape	Loss of epithelial cell polarity and altered epithelial and fibroblast shape in 2D	Growth factor receptors and pathways; cell-adhesion signals associated with cell survival and matrix plasticity
Gene Expression	Cells in 2D versus 3D often have different patterns of gene expression	ECM, hormones, and adhesion molecules

Growth	3D matrix-dependent regulation of cell growth	Adhesion and growth factor-related pathways plus survival or apoptotic genes
Morphogenesis	3D matrix-induced vessel sprouting and gland branching	ECM, adhesion, growth factor-related pathways and apoptotic genes
Motility	Altered single and collective cell motility patterns in 3D matrices	ECM and its regulators; adhesions and growth factor-related pathways; phospholipids
Differentiation	3D matrix-induced cell differentiation	ECM and growth factors; motor molecules

2.2.5 Three-dimensional VIC Cell Culture Models

In vitro 3D systems of VICs are necessary in order to study CAVD mechanisms in an environment with high levels of control (Mabry et al., 2016). Three-dimensional cell culture has become extremely important because it allows for some of the limitations of two-dimensional cell culture to be overcome by more somewhat replicating the *in vivo* microenvironment of the system. Particularly, while working with VICs, controlling their activated/quiescent state is difficult in a 2D environment, yet ultimately subculturing will occur on a plastic plate to get an adequate amount of cells (Roosens et al., 2017). Having a 3D culture system facilitates the intracellular interaction that affects cellular function and mechanisms.

2.3 Improving 3D Models

To further enhance 3D models, more information needs to be gathered on how to create 3D VIC models that have cell aggregation and dynamic stretch.

2.3.1 VIC Phenotypes and Culturing Methods

The majority of VIC's in healthy cardiac valves have a quiescent fibroblast phenotype, yet in a diseased cardiac valve, the majority of the VICs can activate to a myofibroblast phenotype. The myofibroblast phenotype is described as the existence of prominent α-smooth muscle actin (αSMA) stress fibers and are linked to a heightened proliferation, cytokine secretion and even ECM remodeling, When the VIC phenotype is removed and remote from the valve tissue, as well as cultured using a conventional method, it becomes more complex to regulate the VIC myofibroblast phenotype due to the physiological response.

VICs experience osteo-chondrogenic differentiation when grown on a matrix with stiffness similar in degree to that of normal valve tissue (elastic moduli 25–30 kPa) (Hsu et al., 2016). Research from Yip et al shows that when VICs are grown on a stiffer matrix similar to stenotic valve tissue (~113 kPa) myofibroblastic differentiation occurs (Yip et al., 2009). Another mechanism consideration is the effect of TGF-β. Integrins and other proteins associated with mechanical stress influence the release of TGF-β, which affects the phenotype of VICs (Wipff & Hinz, 2008). This explains that when VICs are grown on

substrates that contain certain ECM proteins, such as collagen I, collagen IV, laminin, or fibronectin, the calcification behavior of VICs changes drastically (Rodriguez & Masters, 2009). There are abundant considerations that need to be kept in mind when choosing a medium, in order to ensure the aggregates are not unknowingly manipulated within the hydrogel.

2.3.2 Aggregating Spheroids

When it comes to developing these culture systems, there are different approaches. Roosens et. al. (2017) describes them as two categories: cell-driven without the use of a biomaterial or creating 3D structures by suspending the cells in a biomaterial (usually a hydrogel). For each approach, there are several methods of creation of 3D models or aggregates. In some, the cells will self-assemble without the help of a scaffold, matrix or motion, and this aggregation can be obtained through methods such as the hanging drop method and liquid overlay. Others require some sort of motion that can include but is not limited to centrifugation, rotation or flow of the cell laden media in pellet culture, microfluidics, among others, as can be seen in Figure 8. For the second approach, novel techniques such as encasing cells within photocrosslinkable hydrogels through bioprinting or other methods such as adding a matrix into the media are still a growing and developing field. By being enclosed within a scaffold, the viability of the cells improves greatly and apoptosis is reduced (Ryu et al., 2019).

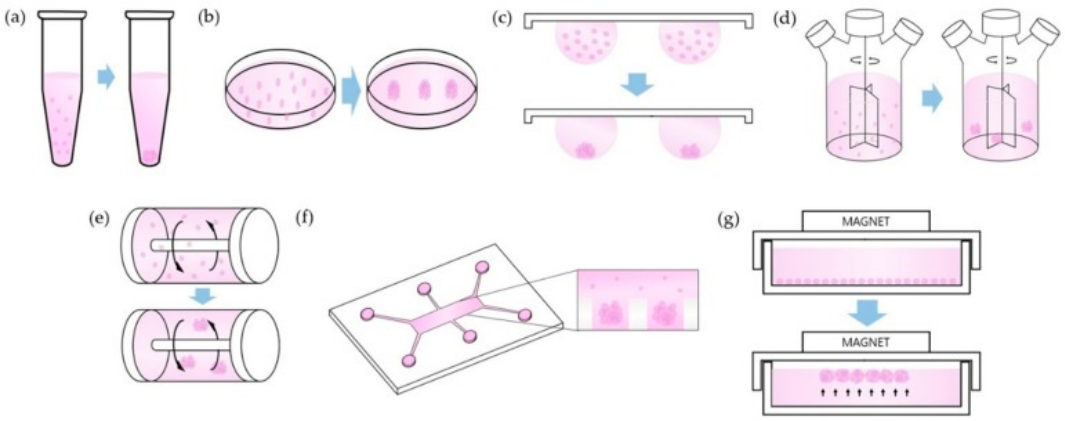

Figure 8: Scaffold-free aggregation methods a) pellet culture, b) liquid overlay, c) hanging drop, d) spinner culture, e) rotating wall vessel, f) microfluidics, g) magnetic levitation [Reported with permission, Ryu et al., 2019]

There are also several different options regarding which cells are used in a 3D cell culture model. Primary cells derived from animal or human explants are the most common, as there appears to be no commercial immortalized cell line to date (Tsang et al., 2018). Most research on aortic valve calcification is performed from cells of large animals (Rutkovskiy et al., 2017). Human primary VIC cells would be the most accurate, but it is difficult to access healthy cells (Bowler & Merryman, 2015). Most human VIC cells used in this application are collected from valve transplant patients meaning they come from diseased valves. Human control cells, meaning healthy human valve cells, can be obtained from a cadaver, but the quality of these cells is lower than those harvested from a living patient (Rutkovskiy et al., 2017). There are other methods of obtaining human control cells that are rare, such as obtaining a heart valve from a heart transplant or other operation that shows no signs of calcification. VICs are not the only relevant cell

type in studying CAVD; VIC and VEC co-cultures have also been used to model valve calcification, considering the role of VEC to regulate VIC calcification (Ruiz et al., 2015).

2.3.3 Scaffolding in 3D Cell Culture

While 2D aggregates are usually grown in monolayers (Figure 9A), three dimensional cell culture aggregates can be grown in two ways: using a scaffold matrix (Figure 9B/C) or in a scaffold-free manner (Figure 9D). Scaffold-based 3D cultures can be generated by seeding cells on an acellular 3D matrix or by dispersing cells in a liquid matrix followed by solidification or polymerization (Edmondson et al., 2014). Commonly used scaffold matrix materials include biologically derived scaffold systems and synthetic-based materials. Scaffold-free 3D cell spheroids can be generated in suspensions by the forced floating method, the hanging drop method, or agitation-based approaches. With each of these methods, cells grow naturally in a 3D environment, allowing cells to interact with each other, the ECM, and their microenvironment (Breslin & O'Driscoll, 2013). These interactions affect a range of cellular functions, including cell proliferation, differentiation, morphology, gene and protein expression, and cellular responses to external stimuli (Shield et al., 2009).

For this application, static methods were chosen due to its simplicity and to avoid the potential introduction of additional variables. A method that was considered was the hanging drop method which is one of the most popular methods of creating spheroids, but the team eventually discarded since it does not allow for high throughput.

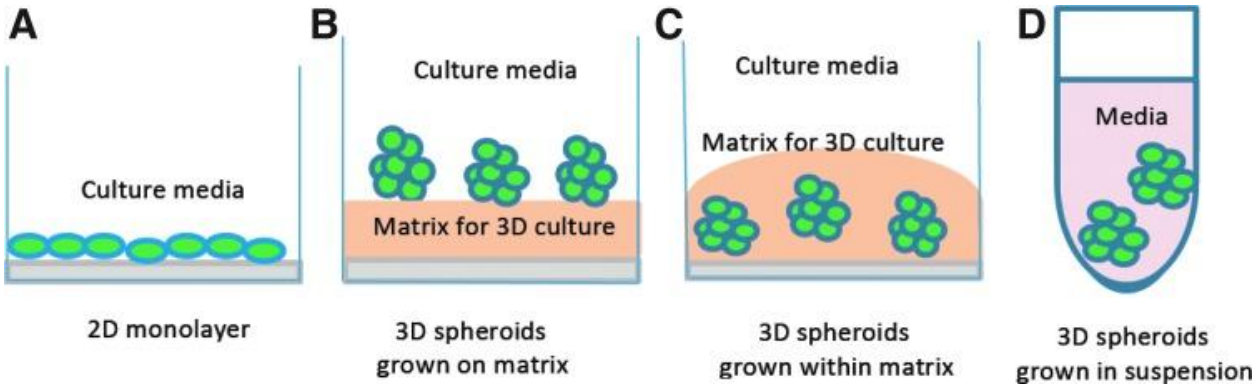

Figure 9 : Schematic diagrams of the traditional 2D monolayer cell culture (A) and 3D cell culture systems: cell spheroids/aggregates grown on matrix (B), cells embedded within matrix (C), and scaffold-free cell spheroids in suspension (D) [Reported with permission, Edmondson et al., 2014]

Encapsulating cells in a biomaterial is usually done through the use of a hydrogel. The most common 3D tissue models utilized for mechanobiological studies are cell-populated collagen and fibrin gels (Kural & Billiar, 2013). In a 3D cell culture setting, the hydrogel is used as a cell carrier when the cellular component is seeded into the polymer meshes or decellularized valve scaffolds (Zhang et al., 2015). The properties of hydrogels allow cells to be embedded within them by mixing cell solution with hydrogel, before the gel formation. Since the cells are embedded in the gel, they have different characteristics than they would in their natural environment (Caliari & Burdick, 2016). Due to this, choosing a hydrogel

specific to the cell culture application is a very important consideration. For example, to model calcification in VICs, the hydrogel needs to consider a range of values - comparing mechanical properties in a healthy aortic valve, mildly calcified valve, and heavily calcified valve (Table 1).

2.3.4 Hydrogel Mediums Currently Used

The current hydrogels used to model calcification with VIC cells can be separated into natural hydrogels and synthetic hydrogels. Natural hydrogels, including collagen and fibrin, are beneficial because they show good bioactivity, however they have poor mechanical durability. Synthetic hydrogels have tunable mechanical properties, but it is difficult to obtain appropriate cell-matrix interactions (Zhang et al., 2015). In past studies, VICs have primarily been cultured in natural hydrogels, such as collagen and fibrin (Benton et al., 2009)**.** These materials provide 3D scaffolds that support cell viability. However, their material properties can be difficult to control. Due to the contractile and remodeling activity of VICs, collagen matrices are quickly compacted by the cells to at least half their original size (Montesano & Orci, 1988). Natural matrices interact with cells by coupling membrane receptors and initiating signaling cascades that direct cell differentiation, proliferation, and migration. As tension increases within a collagen matrix, the mechanisms used by cells to remodel the matrix change. Fibroblasts in the ECM respond differently to growth factor stimulation, depending on if they are under tension or relaxed. The change influences whether cells will acquire an active or quiescent phenotype (Grinnell, 2003).

Some studies completed have focused on utilizing synthetic hydrogels to better understand the mechanical interactions between cells and their environment (Fairbanks et al., 2009). Using photocrosslinkable hydrogels to create a 3D culture system for VICs presents limited damage of encapsulated cells during fabrication and preserves the cell-matrix interaction (Masters et al., 2004).

2.3.5 In-Vitro Mechanical Cell Stimulation

Mechanical stresses in the body can affect regulation of cell formation, function, and development. These mechanical stresses have been noted to potentially affect the development of several diseases, including CAVD. When examining the natural stresses in the *in vivo* hemodynamic environment, there is mainly flow induced fluid shear stress (FSS), and pressure-induced cyclic circumferential strain (CS) (Davis et al., 2015). It's difficult to understand exactly how these stresses work in the body and affect the cells, which is why cell stimulation models are created.

Due to the complexity of the *in vivo* environment, *in vitro* systems have been created to model mechanical stresses. In the general body, These can be categorized based on how they load cells, whether by compression, stretch, bending, or fluid shear stress, or combinations of such (Brown, 2000). Compression tends to be the least relevant in heart valves, considering valves and leaflets primarily undergo the latter three stresses. In valve stimulation, the majority of systems apply a controlled mechanical input, sucha s strain, shear stress, or hydrostatic pressure, then measure the cellular response.

In valves, strain systems simulate the pressure and cyclic strain of the vessel wall due to pulse pressure. Vascular cells contain various receptors that respond to mechanical stimuli. These forces can lead to function changes within cells through signal transduction due to intracellular pathways that are activated by stretch. Strain systems can be broken up into two categories: uniaxial and multiaxial (Davis et al.,

2015). Uniaxial means the system is stressed while multiaxial can stretch in multiple directions (usually two).

Uniaxial stretch is the easiest to model, since it is based on one plane. When the tension is applied to the substrate in this system, there is additional compression in the perpendicular axis (Davis et al., 2015). The advantages of this type of stretch are that it is the easiest to use, and is psychologically relevant to vascular cells specifically. Uniaxial strain models the mechanical effects on smooth muscle vascular cells in the "straight" portion of the blood vessels more accurately (Kurpinski et al., 2006). However, compared to biaxial and multiaxial systems, the data gathered from the strain field is less accurate in this system because it is more difficult to control. There are several devices that do this, all very similar. It typically involves a chamber that a substrate and cells are inputted into and stretched.

Multiaxial stretching provides a more realistic environment, compared to uniaxial, for tissues that typically stretch in multiple directions. However, multiaxial does not necessarily produce a more accurate stimulus, biologically (Bell et al., 2011).

Custom cell stimulation bioreactors are generally used to model both uniaxial and biaxial. A common solution is to culture cells within a flexible substrate. This substrate can then be pulled at a given rate by an actuator by means of posts, clamps, magnets, or it itself being in a flexible mold.

There are also several devices that have been created to model both stress and strain. A device that models multiple stresses is much more accurate physiologically. Two of these systems are: explanted vessels and mock arteries (Davis et al., 2015). The first system takes explanted vessels and connects them to a flow perfusion system. While this device does allow for precise control, the explanted artery needs to be used within a week before severe remodeling occurs (Montorzi et al., 2004). The mock artery system involves creating a tube-like device that has similar properties and dimensions to an actual artery, then perfusing it in a pulsatile flow system. This system applies strain radially, so the stretch experienced by the cells is uniform. However, it is extremely difficult to control individual stimuli.

Chapter 3: Project Strategy

In order to successfully complete the project within the time of the school-year and the allotted budget, the team needed to create a project strategy. This strategy will include the client specifications and goal, detailed objectives to complete the goal, constraints set by the client, design standards, and a management approach outlining the remainder of the project.

3.1 Initial Client Statement

Based on the needs of the client, the team developed the following project goal: to develop a 3D model to study the mechanism of calcification in the aortic heart valve. This client statement was reviewed and later edited through background research and additional constraints that were discovered.

3.2 Technical Design Requirements

After creating a client statement, objectives needed to be established to better understand and prioritize aspects of the goal. In the process of forming objectives, the team needed to take into consideration any potential constraints discovered in the literature review. In the section below, the creation of the objectives, as well as constraints of each will be elaborated on.

3.2.1 Objectives

The objectives for this project were created in collaboration with the client's specifications. These objectives can be seen outlined in the objective tree (Figure 10).

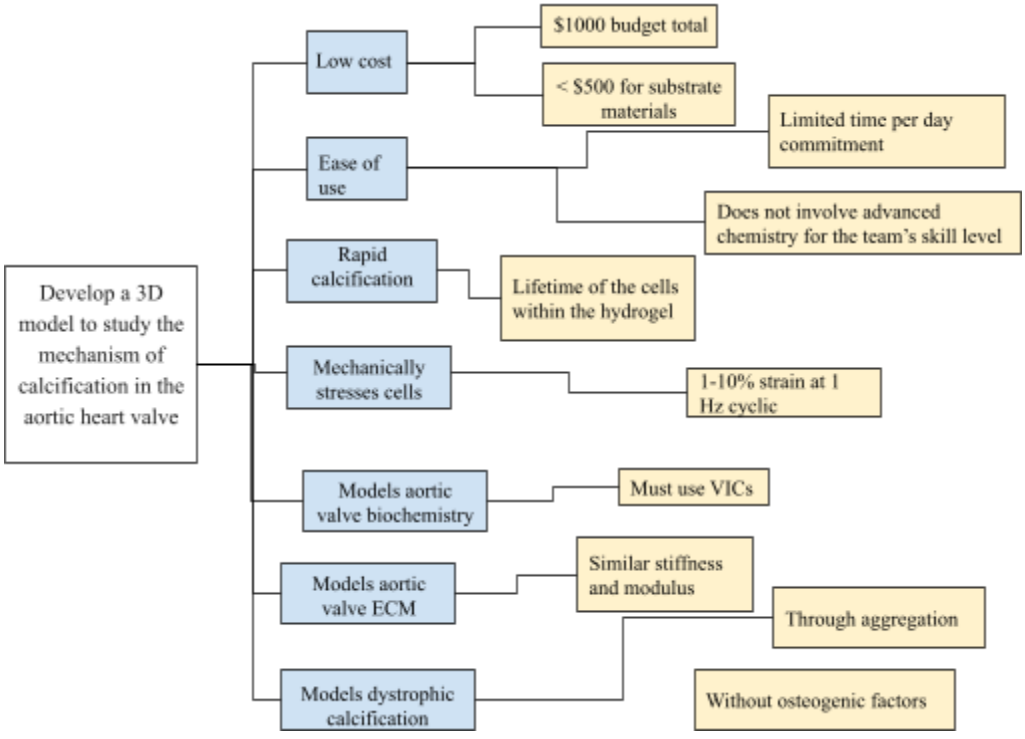

Figure 10: Objective Tree and Constraints

Low cost:
It is important that the materials are of a low cost for this research to be accessible and replicable. Funding constraints are relevant in any assessment of a design, given limited resources.

Easy of use:
The methods used in this study must be easy to understand and replicate to make it easily accessible to other researchers in the future.

Rapid calcification:
This objective will allow the system to calcify quickly. This could be important for the team in terms of time management. If the cells calcify quickly, the team can complete more trials and collect more data than if the calcification time is slow.

Mechanically stresses cells:
The design must include a way to mechanically stress cells without causing cell death. The mechanical stress applied should be similar to what cells experience in the human body, both in a normal heart valve and a calcified one. When the heart is in diastole, cells experience a large amount of tensile stress, which stretches the leaflets about 10%.

Models aortic valve stresses:
The function of mechanical stresses on the aortic valve could be important when designing a 3D model. Given that these are complex, how important this objective is will correlate with how complex the model is. A low ranking of this objective implies that only one aspect of the stresses on aortic valves must be modelled, such as tensile stress.

Models aortic valve biochemistry:
The *in-vivo* environment contains many growth factors and other compounds associated with cell signalling, which affect the function and phenotypic activation of cells. Similar to the previous objective, the completeness of how the design models this aspect is dependent on how important this objective is ranked.

Models aortic valve ECM:
The ECM of the aortic valve plays a role in how the valve handles stress. Collagen fibers, a large component of the ECM, have a particular stress-strain curve as they are recruited and uncrimp, which in turn affects how the cells within the valve are mechanically loaded. Modelling the ECM accurately helps with modelling the stresses experienced by the cells accurately.

Models dystrophic calcification:
The chosen system should promote calcification without requiring the implementation of an osteogenic factor. To do this, aggregation will have to occur and controlled stress must be induced into the system in order to mimic the trauma that is observed in damaged aortic valve tissue and cell death that usually occur before dystrophic calcification is observed in the leaflets.

3.2.2 Constraints

Each of the three objectives comes with constraints that were found in the literature and specified by the client. A chart of these constraints can be seen in Table 2 below.

Table 2: Objective Constraints

Objective	Constraints
Low cost	$1,000 total budget
	< $500 for substrate materials
Easy of use	Does not involve advanced chemistry
	Limited time per day commitment
Rapid calcification	Lifetime of cells within the substrate
Mechanically stresses cells	1-10% stretch at 1 Hz
Models aortic valve stresses	Must be cyclic
Models aortic valve biochemistry	Must use VICs that calcify naturally
Models aortic valve ECM	Similar stiffness to the valve
Models dystrophic calcification	Must calcify, preferably without osteogenic media

Low cost:

Due to having a limited budget of $1,000, the team needs to ensure that the materials are inexpensive to stay under or at the budgeted cost. The team is allotting $500 to the substrate materials since a variety of options will most likely be tested. This budget is based on the allotted amount given from WPI for the project.

Ease of use:

The team is not highly skilled with the materials and methods being worked with, therefore the procedure and materials used need to be of low risk and high success rate. Additionally, the team has a limited time commitment to complete work in the lab, so the procedure needs to be quick and easy to allow multiple trials and have a better chance of obtaining results quickly.

Rapid calcification:

The constraint of this objective is dependent on the lifetime of the cells within the substrate. This timeline will be calculated during the testing phase. The calcification must occur before the cells die inside of the substrate.

Mechanically stresses cells:
One of the constraints of this objective is that the cells must be tested within the substrate between a 1-10% strain at 1 Hz cyclic. These quantities are representative of a heart valve at 60 BPM and mimic a healthy valve. Ideally, the stretch should be extended to up to 15% in order to model a calcified valve, but 1-10% is the baseline goal. A large amount of CAVD patients, approximately 60%, experience high blood pressure with their disorder. As blood pressure increases, there is an increase in stretch. With a 40mmHg increase in pressure, there is a 5% increase in stretch. The system design should be able to model both of these conditions.

Models aortic valve stresses:
The constraint for this objective is merely that it must be cyclic, in order to be representative of the cyclic nature stresses experienced by the heart valve. No electric stresses need be applied, and non-tensile ones also do not have to be considered.

Models aortic valve biochemistry:
The only constraint is that VICs must be used. Other cell types, which would aid in the production of relevant biological signals, are not necessary, nor are any added biochemical factors as they would not provide relevant information regarding the main focus of this project.

Models aortic valve ECM:
Only the range of stiffness and modulus is important when choosing a material to model the ECM. The ability for the cells to adhere and deconstruct the matrix is of little concern, since the aggregation of the cells is more important than their ability to remodel their environment.

Models dystrophic calcification:
The main constraint for this objective is that osteogenic factors are not used to promote calcification mainly to avoid introducing more variables to the system. Additionally, calcification will ideally be obtained through a combination of VICs aggregation and the introduction of stress.

3.3 Design Standards

ISO stands for the International Organization for Standardization which creates standards which guarantee consistency in the quality, safety and efficiency of all products, services, and systems prior to releasing them to the public market (Wilber et al., 2020). Standards are design standards for a product, process, delivery of service or supply of materials that have been created and agreed upon globally by experts in said subject matter (ISO et al., 2021). The standards are formulated by experts based on their knowledge in the matter but also with an advanced understanding of the organizations they represent needs including manufacturers, buyers, customers, sellers users, traders and regulators (ISO et al., 2021). The following standards shown in Table 3 are applicable to the teams model.

Table 3: ISO standards (FDA et al., 2020) (Standards et al 2021)

Standard Number	Title
ISO 20391: 2018	Biotechnology- Cell Counting- Part 1: General guidance on cell counting

	methods
ISO 20391: 2019	Biotechnology — Cell counting — Part 2: Experimental design and statistical analysis to quantify counting method performance
ISO 10933-I:2009	Biological Response Resulting from Device Mechanical Failure- specifically excludes biological hazards arising from any mechanical failure,

3.4 Final Client Statement

Based on the needs of the client and information found in the Literature Review, the team developed the following revised project goal: to develop a 3D *in-vitro* model to study the mechanism of valvular interstitial cell (VIC) dystrophic calcification under mechanically dynamic conditions.

3.5 Management Approach

The team plans to approach our project by following the timeline of our gantt chart to ensure all of our tasks are completed in a structured, timely manner. During the first two weeks of B term the team plans to finalize the drafts for the Introduction, Literature Review, Project Strategy and Design Process sections, to fully prepare the team for the laboratory portion of the project. In B term the team is focusing on the strategy, design process and design validation for the wet lab. In C term the team plans to analyze, validate and verify the data the team collected in B term. With this information, The team will work to create the drafts for the Discussion, Project Impact and Conclusion sections of the report. For the last term of the project, D term the team plans to finalize the full report, complete a poster showcasing the teams research, data and conclusions, as well as do a final presentation.

Table 4: Gantt Chart

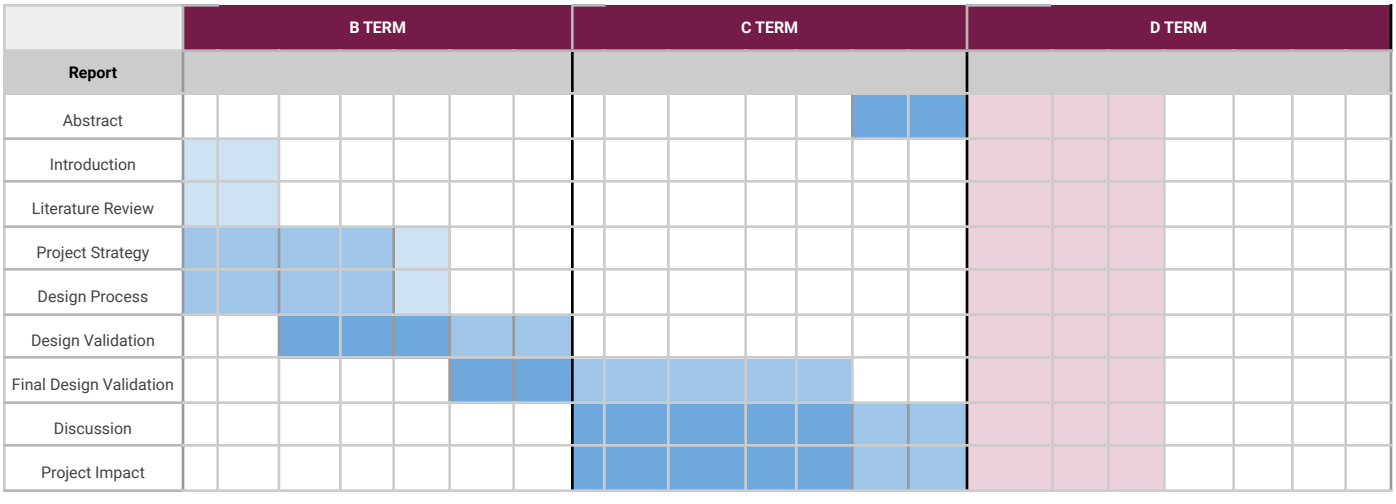

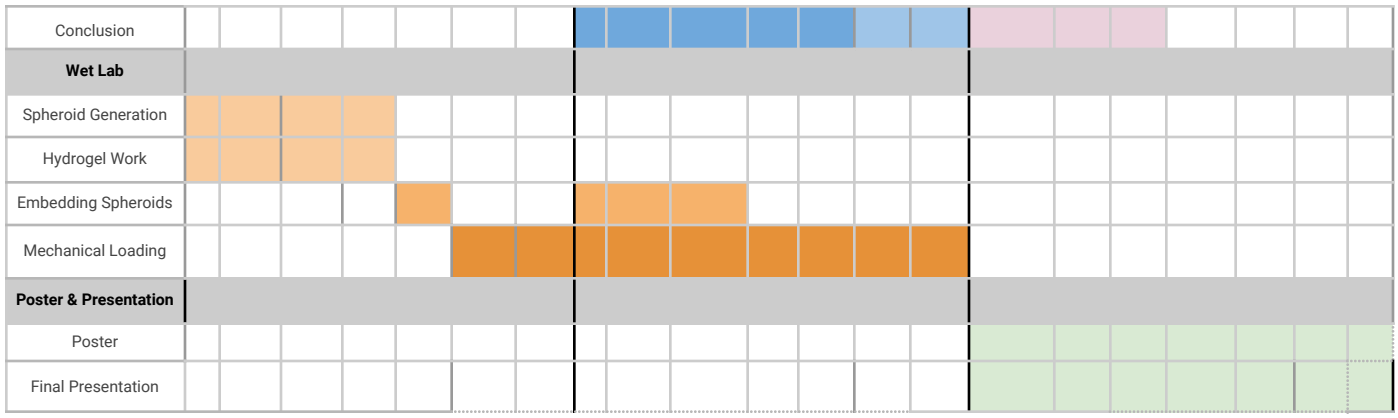
Conclusion
Wet Lab
Spheroid Generation
Hydrogel Work
Embedding Spheroids
Mechanical Loading
Poster & Presentation
Poster
Final Presentation

Chapter 4: Design Process

This chapter explains the design process throughout the project. It will explain the overall objectives the design needs to meet, include a function means table, and will expand on several design concepts. At the end of the chapter, a final design concept is selected based on if they meet the objectives of the project.

4.1 Needs Analysis

The following section outlines comparisons of individual objectives and specifications and ranks their importance based on the client's needs.

4.1.1 Pairwise Comparison of Objectives

Following several client interviews, the team determined the major needs and wants of the client. In order to ensure that the major needs of the client were met, a pairwise comparison was used to rank the individual objectives of the overall design in Table 5.

Table 5: Pairwise Comparison of Objectives

	Mechanically stress cells	Models the aortic valve biochemistry	Models the aortic valve ECM	Models the aortic valve stresses	Models dystrophic calcification	Easy use	Rapid calcification	Low cost	TOTAL
Mechanically stress cells		1	1	1	0	1	1	1	6
Models the aortic valve biochemistry	0		0	0	0	0	0	0	0
Models the aortic valve ECM	0	1		0	0	1	1	1	4
Models the aortic valve stresses	0	1	1		0	0	0	0	2
Models dystrophic calcification	1	1	1	1		1	1	1	7
Easy use	0	1	0	1	0		0	1	3
Rapid calcification	0	1	0	1	0	1		1	4
Low cost	0	1	0	1	0	0	0		2

Based on this table, the team was able to rank objectives from most important to least important. This will be beneficial when decided on a final design concept to pursue. The ranking of objectives (from most important to least) is as follows: models dystrophic calcification, mechanically stresses cells, models the aortic valve ECM, rapid calcification, easy use, low cost, and models the aortic valve biochemistry.

4.2 Design Components

The team's design must meet all the objectives described in Table 3. If not all objectives are attainable, the design should be chosen based on the most important objectives described. In Chapter 3, each objective's constraints were described. All of the constraints for each objective considered needs to be met in the final design.

4.2.1 Function Means Table

In order to begin conceptualizing possible means of achieving various specifications requested by the client, a functions means table was created (Table 6). The two main functions of the design were selected to be mechanically stresses cells and models dystrophic calcification. These functions were chosen since they were ranked most important, as seen in Table 6. Each of these functions was then broken down into various specifications as clarified by our objectives tree in Figure 7.

Table 6: Function Means Table

Function	Specification	Means
Mechanically stresses cells	1-10% stretch at 1 Hz	● Uniaxial stretch ○ CellScale MCFX ● Biaxial stretch ○ FlexCell FX4000 ● Valve pump ● Bending
Models dystrophic calcification	Must calcify, preferably without osteogenic media	● Test with alazarin crimson stain ● The mechanical stress will trigger dystrophic calcification.

4.3 Potential Design Concepts

Based on the design objectives, three design concepts were created.

4.3.1 Design A: Aortic Valves in Left Heart Simulator

When thinking about modelling aortic valve calcification, one way is to harvest aortic valves and mechanically stress them. Porcine valves would be fitted into a left heart simulator that would exert pressure on the valve comparable to that in the heart valve (Figure 11).

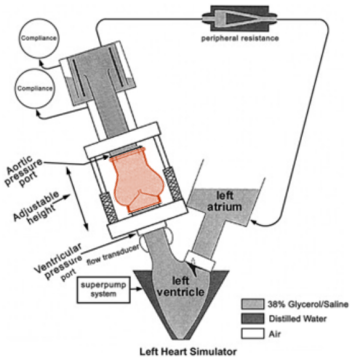

Figure 11: Design concept: aortic valve in left heart simulator
[Reported with approval, Travis et al., 2009]

The valve, and therefore the cells, would be mechanically stressed by the pressure in the pump. Dystrophic calcification could be modelled by the addition of cytokines to promote cellular aggregation within the valves However, calcification is not necessarily guaranteed in this model. Notably, this is not a particularly easy or low cost option. A device to apply the pressure to the valves would have to be either bought or created. It does, however, model the biochemistry, ECM, and stresses of the valve very well, considering it is an entire valve *ex vivo*.

4.3.2 Design B: VICs Seeded in Hydrogel in Pressure Chamber

A more controlled option would be to still use chemical signalling to cause aggregation, but seed VICs into a hydrogel (Figure 12) and mechanically stress them via a pressure chamber fitted with a pulse generator that could apply cyclic stress.

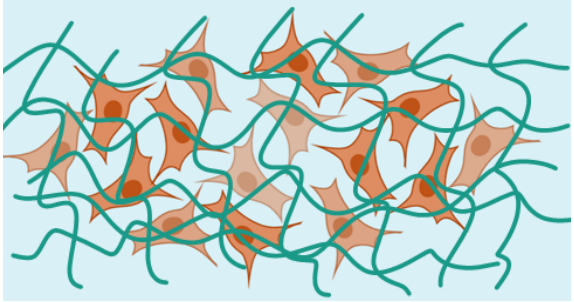

Figure 12: VICs seeded in a hydrogel. Made with BioRender.com.

An example of a pressure chamber being used to cyclically stress aortic valve leaflets is shown in Figure 13. This could theoretically be used in any stress device. The aggregate plate will be placed into the chamber which then is placed in an incubator or under a microscope. A vacuum tube is inserted and CO2 levels can be monitored with a sensor device. This system will be fully automated for gas exchange to ensure optimal cell viability. Though the system can mimic hydraulic pressure, it is not necessarily controlled stretch.

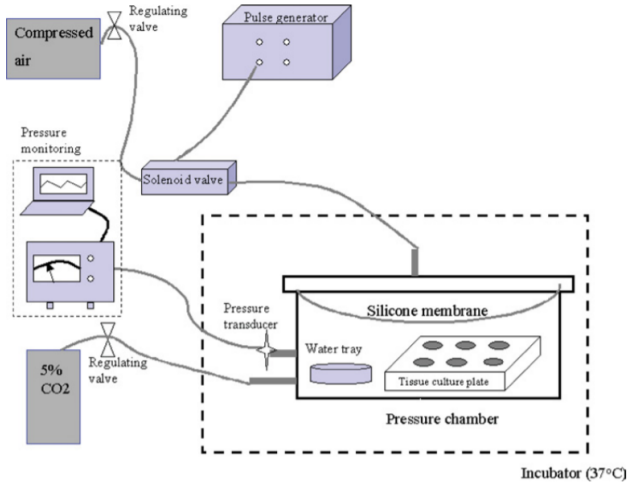

Figure 13: Cyclic pressure chamber
[Reported with approval, Xing et al., 2004]

While this is a lower cost and higher throughput option than design A, it also suffers from being more difficult to use due to the fabrication of the pressure chamber.

4.3.3 Design C: Embed Spheroids into a Hydrogel

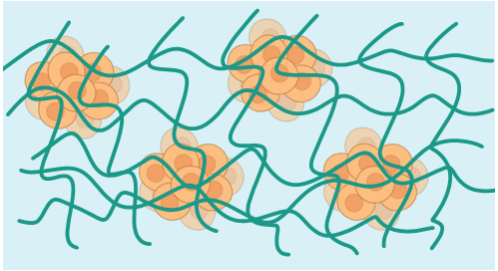

Figure 14: Spheroids embedded in a hydrogel

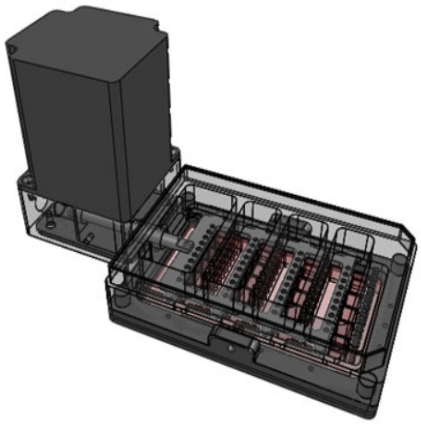

Figure 15: CellScale MCFX
[Reported with approval, Zeugolis & Amsden, 2020]

This design involves creating spherical VIC aggregates, embedding them into a stretchable hydrogel, and applying tensile stress to this system. By forming aggregates before mechanically stressing the cells, the need for growth factors is eliminated while still effectively modelling dystrophic calcification. Using a tensile testing system found within our lab decreases the cost significantly, when compared to the other options, and it also increases ease of use given the training that others in the lab already have.

4.4 Final Design Selection

After discussing each design, there are many benefits and deficits to each. In order to ensure the most viable design is chosen, each design was compared to the list of objectives the team created. This comparison can be seen in Table 7. The objectives are ordered relative to their importance, as determined by the pairwise analysis; ranks are shown on the left, since some were ranked equally. A higher number indicates higher importance. If the design can satisfy the objective, it will be marked with a check; if it cannot, it will be left blank. Designs which have the potential to satisfy an objective have been marked

with a question mark. Whichever design has the most checks higher up on the chart is the best suited for the team's project.

Table 7: Design Selection

Rank	Objective	Aortic Valves in a Left Heart Simulator	VICs in Hydrogel in Custom Pressure Chamber	Spheroids in Hydrogel in Available Tensile Testing System
7	Models dystrophic calcification	?	✔	✔
6	Mechanically stresses cells	✔	✔	✔
4	Rapid calcification	✗	?	✔
4	Models aortic valve ECM	✔	✗	✔
3	Easy use	✗	✔	✔
2	Low cost	✗	✔	✔
2	Models aortic valve stresses	✔	✗	✔
0	Models aortic valve biochemistry	✔	?	?
N/A	Allows for imaging	✗	✔	✔

Once the team progressed further into the course of the project, they realized being able to image the cells is a large part of the system validation. Because of this, imaging was added as an objective but not included in the ranking system.

Our final design concept is to create spheroids within agarose micro-chambers and embed these into a hydrogel. The spheroid creation method is within the ultra-low attachment category and enables us to create a variety of different sizes at a consistent density by changing the size of the wells. The spheroids will then be mixed in a prepolymer solution and crosslinked via a cytocompatible method, such as light or temperature within a suitable range.

4.4.1 Final Design Objectives and Constraints

Once the final design was chosen, this design concept was broken up into three objectives. Following several client interviews, the team determined the major needs and wants of the client. The objectives are as follows:

Objective 1: to consistently form spherical VIC aggregates of a specific size
Objective 2: to produce a stretchable hydrogel in which the spheroids can be embedded

Objective 3: to apply tensile stress to the spheroid-laden hydrogel

In order to ensure that the major needs of the client were met, a pairwise comparison was used to rank the individual objectives of the overall design in Table 7. From this table, the team learned that the most important objective is objective 1, followed by objective 2, and lastly objective 3.

Table 8: Objective Pairwise Comparison

	Objective 1	Objective 2	Objective 3	Total
Objective 1		1	1	2
Objective 2	0		1	1
Objective 3	0	0		0

Each of the three objectives comes with constraints that were found in the literature and specified by the client. A chart of these constraints can be seen in Table 9 below.

Table 9 : Objective Constraints

	Constraints				
Objective 1	Not too large	Creates consistent sizes	Range of sizes possible	Short formation time	High throughput
Objective 2	Not cytotoxic	Not impermeable by media	Remodelable/ biodegradable	Adheres to wells	Range of stretch, and elastic modulus
Objective 3	Does not ravage the hydrogel	Does not “pop out”	1-10% stretch standard	Uniaxial testing	Can model a range of stretch, elastic modulus, and stiffness

These objective constraints, in addition to others, were later separated into two categories: creating aggregates and creating a hydrogel. These constraints were presented to the client and put in a pairwise analysis to rank importance. These analyses can be found in Appendix C.

4.4.2 Final Design Approach Refinement

The first step, to create aggregates, involves several concepts that need to be considered: shape, size, cell amount, and formation time. Spheroids are an ideal shape to consider because there is evidence that when looking at calcified nodules in a 2D format, circular cross sections are observed; this means the nodules are presumably spherical (Rodriguez et al., 2009). When looking at size, there are many size references in literature with spheroid sizes ranging from approximately 50 to 400 micrometers. The aggregates need to be at least 100 micrometers in order to be considered aggregates and no larger than 200 micrometers to

avoid necrosis (Fisher et al., 2013). The number of cells between will be about 600 to 2,000 because this range gives the optimal number of cells to avoid dense central regions that cause disaggregation. The formation time of the aggregates will be less than 6 days for the purpose of media replenishing.

In order to create spheroids, there are three methods that can be used. The first method was the hanging drop method where cell laden media is dispensed into the crevices of a 96-well hanging drop plate and after some time, the cells will form into a spheroid at the bottom of the hanging drop. The second method includes culture media supplemented with MC. That, in addition to utilizing ULA plates, will allow for the aggregates to form with a MC matrix that is inert and does not have growth factors that could affect the VICs. And lastly, for the third method, non-adhesive ultrapure agarose microwells would be fabricated by using a PDMS master as a mold in which the team could dispense an agarose solution that after solidifying, can then be removed and put into a culture plate where it can be loaded with the cell solution.

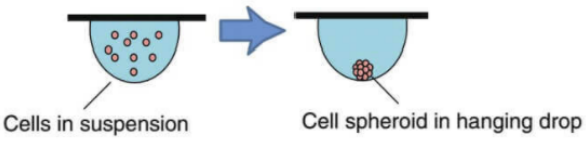

Figure 16a: Hanging drop method [Reported with approval, Breslin & O'Driscoll, 2013]

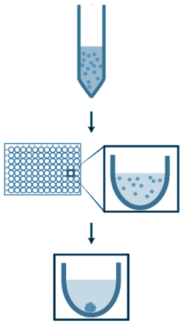

Figure 16b: ULA+MC [Reported with approval, Maritan et al., 2017]

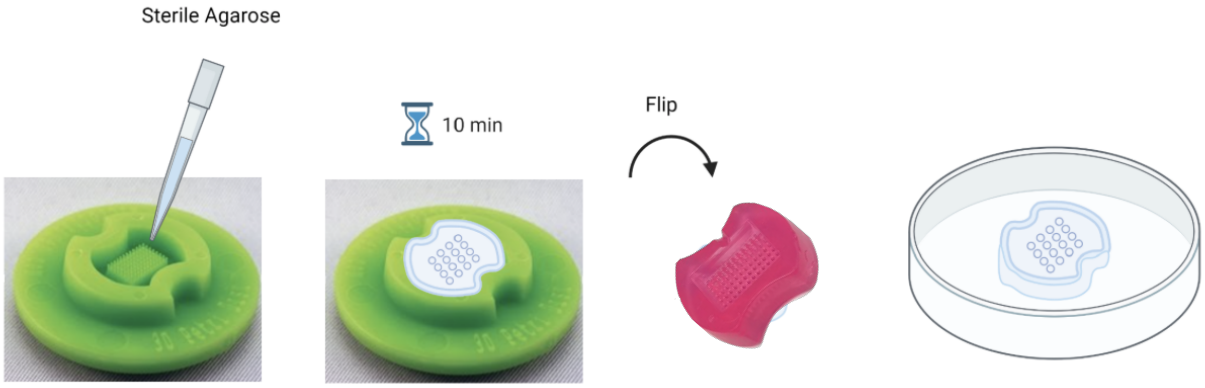

Figure 16c: Agarose microfabricated wells

Each of these methods have advantages and disadvantages. With the hanging drop method, spheroids cannot be easily monitored during formation, which would not allow for good size control of the aggregates. Additionally, in order to be able to test the spheroid, it must be transferred and this can cause disaggregation. For the second method, size can be determined by modifying the MC concentration but too much or too little could result in aggregates that are too loose or that present with formation of cell

monolayers. Lastly, one of the major advantages of the third method is that the size of the aggregates is highly reproducible and easily adjustable to whatever the client needs. Additionally, since the client specified that the implementation of additional chemicals was not a topic of concern, the culture medium would be supplemented with AA (ascorbic acid). By doing this, VICs will aggregate and the AA will keep the aggregates alive by avoiding densification of the central regions that causes aggregate degeneration. A compiled list and pairwise analysis of aggregate creation constraints can be found in Appendix C. Based on all of the information found, each method was compared to the requirements in a table to choose the best option. Table 10 shows that the best option for the team's application is the agarose microfabricated wells.

Table 10 : Aggregate Creation

	Requirements (Roosens et al., 2017)	Hanging drop 96-well plate (Bresciani et al., 2019)	ULA 96-well plates and MC matrix (Maritan et al., 2017)	Microfabricated chambers (Roosens et al., 2017)
Size of aggregates	100 - 200 µm	~200 µm	200-500 µm	Adjustable: 150-110 µm in 400 µm wells
Number of cells	~600-2000	~2400	~1000	~629 for 150-110 µm spheroids
Aggregate formation time	<9 days	3-6 days	24-48 hours formation 5-10 days	24 hour formation 3 days
Notes	N/A	Hard to maintain culture, change media, and monitor spheroids	Inconsistent sizes and densities	Customizable, large range of sizes possible

Once the speroids are created, they will be embedded into a hydrogel. Hydrogel matrices are composed of natural and synthetic polymers held together by physical and chemical crosslinks. A hydrogel must be photo- or thermally crosslinked to embed spheroids without cytotoxic effects. Spheroids will be mixed with a liquid precursor to a hydrogel and light or heat would be applied to form the gel. Hydrogels are commonly used because of their high water content, which allows the distribution of media in 3D cell culture. Many are biocompatible and can be adjusted to match the environment of the natural tissue. Important considerations when selecting a hydrogel is its adhesion and stretchable properties. Natural hydrogels have native adhesive properties, where synthetic gels generally need to be modified to fit this requirement. When choosing a hydrogel, it should model a range of modulus from a healthy aortic valve (7 kPa) to a calcified valve (950 kPa) (Wang et al., 2012). It should also have bioinert properties so it will be easier for the cells to attach to. Hydrogels should be easy to prepare due to both time constraints and skill levels. A compiled list and pairwise analysis of hydrogel creation constraints can be found in

Appendix C. The hydrogel should also have adhesive abilities in order to mechanically load the hydrogel. Potential hydrogels and their properties are outlined in Table 11 based on the constraints discussed in table 8: range of modulus, remodelable/biodegradable, adhesive, not cytotoxic, as well as cost.

Table 11: Hydrogel Creation

	Modulus (Litvinov & Weasel, 2017) (Wu et al., 2019) (Duchi et al., 2017)	Remodelable/ Biodegradable	Adhesive (Li et al., 2015) (Assmann et al., 2017)	Not cytotoxic	Cost
Requirements	~7-950 kPa (range of healthy to calcified valve)	✔	✔	✔	< $500
Fibrin	~16 kPa (20 mg/mL concentration	✔	✔	✔	N/A (in lab)
Collagen	~12 kPa (9 mg/mL)	✔	✔	✔	$175 for 100 mg (Corning)
Agarose	~275 kPa (25 g/L concentration)	✔	✗	✔	$198 for 100 g (ThermoFisher)
GelMA	~35 kPa (at 10% concentration)	✔	✔	✔	$135 for 1000 mg (Adv. BioMatrix)
HAMA	~92 kPa (at 10% concentration)	✔	✔	✔	$240 for 100 mg (Adv. BioMatrix)
PEG	~0.8 kPa (at 20% concentration)	✗	✔	✔	$173 for 100 mg (Sigma Aldrich)
Polyacrylamide (PAM)	~6.8 kPa (at 10% acrylamide and 0.03% of bis-acrylamide	✔	✔	✗	$90.70 for 10 g (Sigma Aldrich)
GelMA+HAMA co-gel	1.5±0.4 to 73.0±11.1 kPa (at 1-10% GelMA and 0-2% HAMA)	✔	✔	✔	$349 a kit, including Igracure (Sigma Aldrich

To ensure the viability of the data found in the literature, a rheometer test will be completed at the concentrations used in the final protocols.

Automatically, the PEG, PAM, and agarose are no longer viable for consideration based on the material properties. PEG, along with not meeting the modulus range, is cytotoxic and not safe for embedding spheroids. PEG can be tuned over a wide range to meet more of the requirements, however it can't be

used for a 3D system, only 2D. Agarose, though it seems like a good fit, does not have good adhesion properties so it would not be able to stretch the spheroids properly. Going forward, fibrin, collagen, GelMA, HAMA, and the GelMA+HAMA cogel were compared. The mechanical properties in the table above are variable based on each gel. For this reason, rheology needs to be completed during the lab to compare a uniform test on each gel to obtain a fair modulus.

Once cells are embedded, they are stretched. The CellScale MCFX device can stretch the gels uniaxially with a maximum strain of 12.5% (Figure 17). The spheroids adhere to posts that stick out from the bottom of the single use silicon well plate. Then the user can specify the stretching protocol done to the well plate, and this protocol will stretch the cells in a linear direction. The device has a single monolayer configuration with 8 wells, 8x8 mm. The maximum cycle frequency is 30 Hz and the maximum load is 30 N.

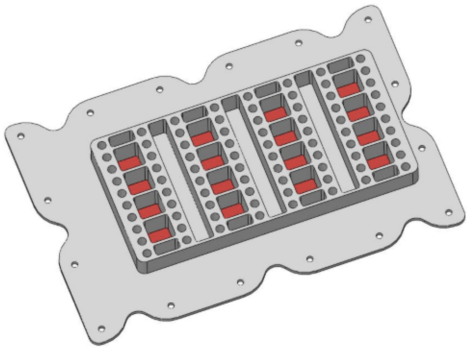

Figure 17: MCFX CellScale plate [Reported with approval, Zeugolis & Amsden, 2020]

Chapter 5: Design Validation

This chapter expands on each aspect of the chosen design. Each design aspect was validated based on objectives ranked by the clients.

5.1 Design Overview

The chosen design can be broken down into four components: aggregate creation, hydrogel creation, embedding cells, and stretching. The methods and initial validation of each aspect will be discussed through the chapter. In order to ensure that the selected design can be effective and meet all the client's requirements, preliminary testing was conducted. Each of the four components was tested separately. Once the team can receive accurate data from the individual components, they will be tested in unison for actual data collection and analysis.

5.2 Aggregate Creation

The team chose a protocol described by Roosens et al (2017) in which non-adherent ultrapure agarose micro-wells are created by dissolving the sterile agarose powder in PBS, heating it and pouring the liquid solution into a custom made negative polydimethylsiloxane PDMS(-) master and left to solidify. Once they have cooled, they can be removed from the mold and transferred into cell culture plates.

In order to obtain spheroids, seeding 1×10^6 VICs into the micro-wells is required. In this way, the cells will form spherical aggregates that can then be imaged and retrieved for further testing. The complete protocol for aggregate creation is attached in Appendix D. The images in Figure 18 were obtained by Colin Coutts and are as follows: Image A is of a brightfield in which the spheroid being analyzed can be observed clearly; Image B and C represent stains that were used to assess viability and apoptosis. Propidium Iodide is not permeable to live cells and as such, it is able to detect dead cells in a population. Caspase is a marker of programmed cell death also known as apoptosis, that has been demonstrated to precede calcification in *in-vitro* models.

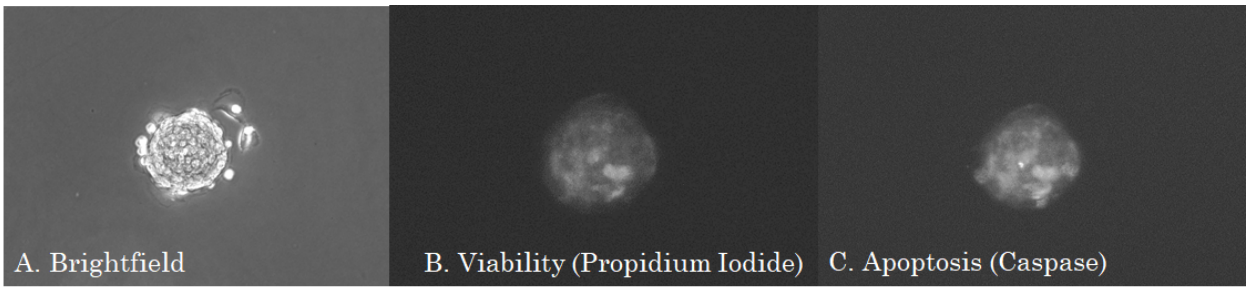

Figure 18: Images of aggregates
18a: Staining of spheriod allowing for full analysis and clarity
18b: Spheriod stained for viability, determine cell health
18c: Staining of spheriod to assess apoptosis of the cell or cell death
. Obtained from Coutts, C. (2021)

5.3 Hydrogel Medium

After outlining various hydrogel medium options in Table 11, three different hydrogels, collagen, fibrin, and a combination gel made up of gelatin methacrylate and hyaluronic acid methacrylate (GelMA + HAMA) were selected for preliminary testing according to their unique material properties. A table summarizing these properties can be seen below (Table 12). The protocols for each individual gel are discussed in this section.

As discussed in the previous chapter, both fibrin and collagen were viable options to use as gels. Fibrin has natural wound healing properties that is used commonly to model damage in the body. Collagen is the main component of the ECM and valve leaflets, so it would be an accurate model based on material properties. However, both of these options allow for cell migration. The concentrations at which the hydrogels were created are as follows: Collagen hydrogel at ~2.03 mg/mL, Fibrin hydrogel at 6.68 mg/mL of fibrinogen and thrombin at 2 units per mL in the final solution. These concentrations are broadly used in the creation of hydrogels used as matrices in cell culture and experimentation.

Based on the literature from Hjortnaes et al. (2014), the GelMA+HAMA co-gel was chosen over the individual GelMA and HAMA gels.When comparing 1% and 2% wv HAMA, with 5% and 10% wv GelMA, the GelMA retained the most live cells over the course of 21 days. However, when comparing the co-gel to the individual gels, the co-gel with 1% wv HAMA and 5% wv GelMA contained the most live cells after 21 days, approximately 90%. The graphical data can be seen below in Figure 19. In addition to successfully being embedded with cells, the co-gel is also synthetic and highly controlled, so it's properties can be easily manipulated. However, though it is synthetic it is not biomimetic.

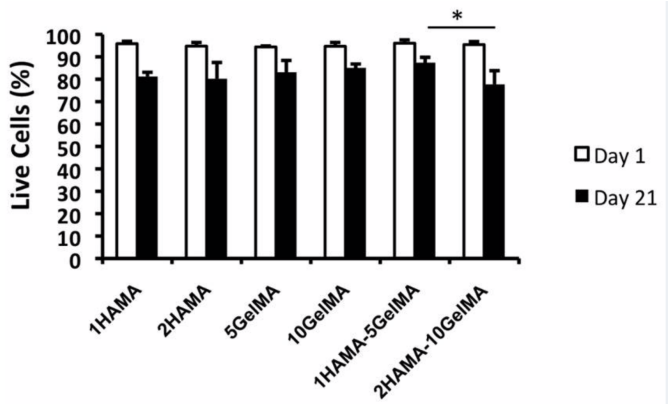

Figure 19: GelMA, HAMA, and GelMA+HAMA Concentration Comparison [Reported with approval, Hjortnaes et al., 2014]

Table 12: Pros and Cons of Hydrogel Options

	Pros	**Cons**
Fibrin	Wound healing, appropriate for	Degradable by cells, allows for

	modeling damage	migration
Collagen	Main component of ECM	Degradable by cells, allows for migration
GelMA+HAMA	Synthetic, controlled	Not biomimetic

In order to further understand the material properties of fibrin, collagen, and GelMA+HAMA, an oscillation stress sweep test was proposed to be conducted on the rheometer. Unfortunately, due to technical errors, the rheometer was unavailable for testing and the properties of the gels could not be directly verified.

To ensure each gel would be able to complete a 7 day trial of stretching without popping out of the CellScale wells, the gels were tested without any embedded aggregates. After several trials, the team found that in order to stay hydrated, fibrin and collagen needed to be hydrated a minimum of 80 μL every other day, while GelMA+HAMA needed to be hydrated 80 μL every day. These "empty" gels were hydrated with DPBS, while gels with aggregates were hydrated the same amounts with complete media.

5.3.1 Collagen

In order to test creating a collagen gel, a protocol was modified from Charoen et al.. The final protocol for the gel can be found in Appendix E. It involves combining a 50/50 ratio 4.07 mg/mL Rat Tail Collagen Type 1 solution with 5x DMEM to help the cells thrive. The entire protocol should be completed over ice.

This part of the trial was completed in the 8x8mm well-plate for the CellScalem with a 3mm depth. The solution did polymerize after benign incubated for an hour and was the correct consistency. The color for the gel was bright pink, but this was due to the high concentration of phenol red in the 5X DMEM (Figure 20).

Figure 20: Collagen gel in CellScale plate

5.3.2 Fibrin

The second hydrogel that was produced was a fibrin gel. The complete protocol for its creation can be found in Appendix F. The gel is composed of a 16.7 mg/mL fibrinogen stock solution and a 25 unit thrombin stock solution. When not in use fibrin should be stored in the -20°C freezer and thrombin should be stored at -80°C. Thrombin is extremely sensitive to temperature and will thaw with handling alone

while fibrinogen can be thawed in a water bath when working in non-sterile environments. Once cells are introduced into the system, alternate methods must be sought in order to keep a sterile environment.

To obtain the desired concentration of fibrinogen and thrombin, DPBS had to be used to dilute the stock solutions to 6.68 mg/mL and 2 units per mL respectively. Once they were diluted, fibrinogen and thrombin were very gently mixed in equal parts, avoiding bubbles, and incubated at 37°C for at least an hour or overnight.

The first time this method was attempted, 1 mL of each individual solution was made and once they were mixed, the fibrin hydrogel solution was distributed in 160 µL quantities into the wells of an 8-well strip and left to incubate at 37°C. Once gelation had been confirmed and the protocol verified as effective, the procedure was repeated inside the 3mm well-plate of the CellScale, as observed in the two right wells on Figure 21, with modified quantities.

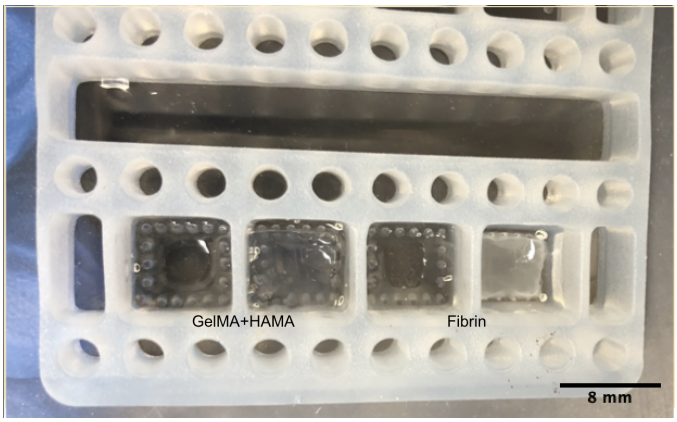

Figure 21: Fibrin (right 2) and GelMA+HAMA (left 2) gels in CellScale plate

5.3.3 GelMA +HAMA

Based on the work of Hjortnaes et al. (2015), the team pursued the production of a gelatin methacrylate and hyaluronic acid methacrylate cogel. Unlike the collagen and fibrin gels, which polymerize given an hour at 37 °C, the methacrylation allows one to utilize a chemical crosslinker that is initiated by UV light. Irgacure was selected as the crosslinking material for this gel. This is effective within 30-90 seconds of UV light exposure at 2.5 mW/cm2 power, which is a short enough duration to ensure cell viability. All precursors and the photoinitiator are stored in refrigerated or frozen conditions before use, and heat must be applied to dissolve the components in a buffer solution for which PBS was selected. This can be done in an oven or on a hotplate, and evaporation of the buffer solution should be minimized. The complete protocol can be accessed in Appendix G.

This procedure was successfully performed once to confirm effectiveness and a second time inside the well-plate of the CellScale (3mm depth), as observed in the two left wells on Figure 21, with the same ratios. The ratio of materials in this co-gel can be modified to better fit the needs of this project in the future.

5.4 Embedding Spheroids Statically

While there is some concern over exposing spheroids to excessive shear stresses, micropipettes are suitable for picking up and transferring spheroids (Han et al., 2015). The agarose mold was inverted onto a 60 mm tissue culture plate. The aggregates were then picked up with micropipettes and were placed in a well with the prepolymer solution. The gels can then be allowed to polymerize, either through UV radiation for 90 seconds or incubation at 37°C for one hour. This method, while accurate, was extremely difficult to conduct and time consuming.

In order to attempt simpler aggregate placement and less stress to the aggregates as a whole, a secondary method was attempted. Similarly to the initial method, the agarose mold was inverted onto a 60mm tissue culture dish. From here, the plate was rinsed and the aggregates were suspended in complete media. The pre-polymer solution was then created, and the aggregates were picked up with a micropipette and placed with the unmixed pre-polymer solution. The solution was then pipetted up and down to mix the aggregates and the gel solution. Then the pre-polymer aggregate combined solution was pipetted into the CellScale microwells. The gels can then be allowed to polymerize, either through UV radiation or incubation at 37°C for one hour.

Initially, this method failed because a coated tissue culture dish was used. This caused the aggregates to stick to the plate and they were unable to be removed. This was attempted again with a non-coated dish and aggregates were successfully embedded into a collagen gel. These aggregates were embedded into a static gel to see the natural reaction between the gel and aggregates without stretching.

This method was successfully completed and aggregates were embedded into all three gels, collagen, fibrin, and GelMA+HAMA. Each gel was initially tested for a 4 day period, with aggregates embedded statically. This time period was chosen since the literature shows there are signs of calcification 1 day after embedding, and because of the timeline of the project.

Aggregates embedded in collagen showed signs of great cell viability. The aggregates attached themselves to the hydrogel and became embedded with the movement of the fibers. Over the course of all four days, there were no signs of migration and the aggregates remained mainly intact.

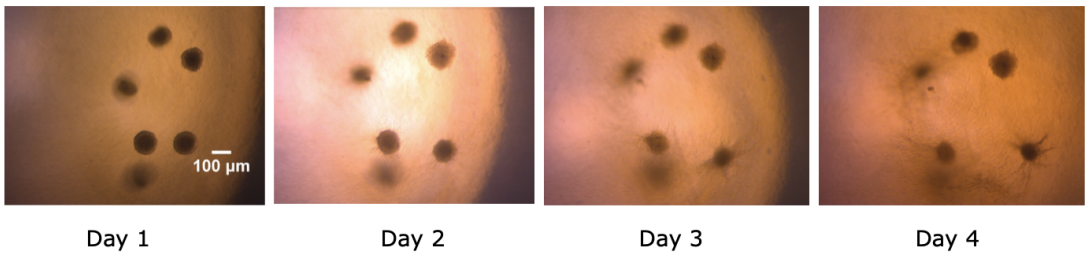

Figure 22: Collagen Embedded Aggregates (4x magnification)

Over the course of the trial, the fibrin-embedded aggregates showed signs of movement each day. On day 2 they migrated closer together, then were touching on day 3. However, the next day each aggregate moved to the opposite side of the well. However, as shown below, there were signs of migration

beginning on day 2 (Figure 23).

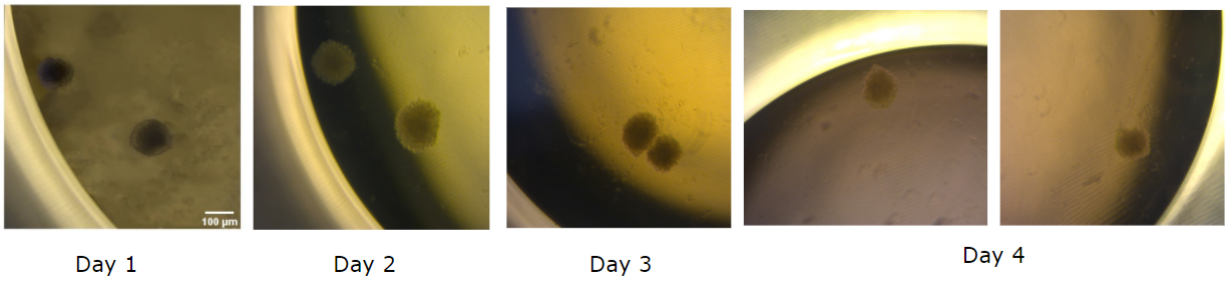

Figure 23: Fibrin Embedded Aggregates (10x magnification)

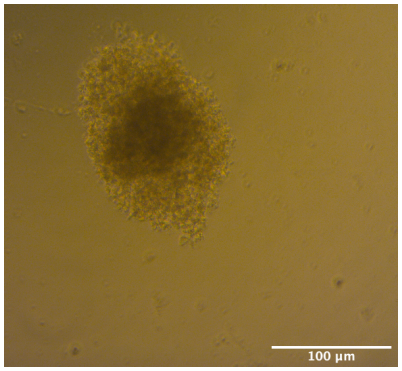

Figure 24: Migrated Aggregate into the Fibrin Matrix- Day 2 (20x magnification)

While embedded in GelMA, the aggregates remained intact for the entire period. There were little signs of movement and no signs of migration or disaggregation.

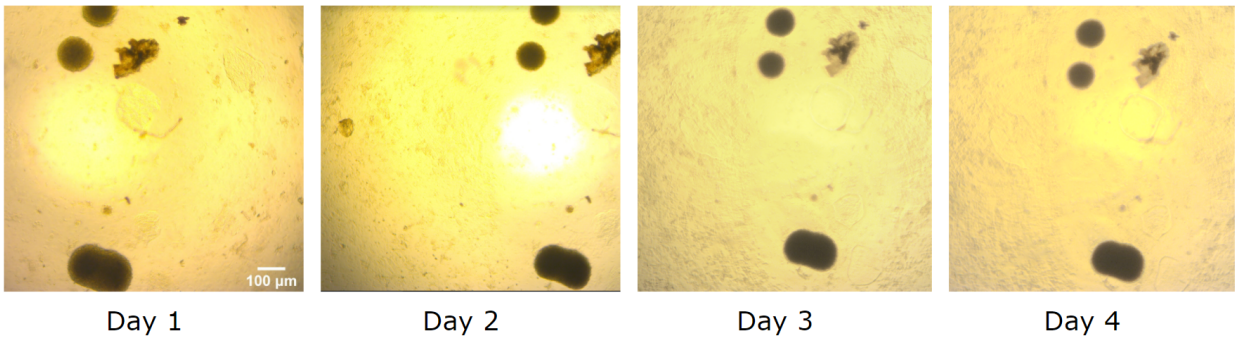

Figure 25: GelMA+HAMA Embedded Aggregates (10x)

5.5 Stressing Embedded Spheroids

After embedding aggregates into three hydrogels statically, aggregates were embedded into the same gels in the CellScale. These aggregates were stretched over the course of 7 days to see how stressing affected the integrity of the aggregates and system.

Figure 26: Collagen Embedded Spheroids in CellScale (10x).
The dark area on day 3 is a post of the wellplate.

In collagen, there were no signs of disaggregation. On day 4, there appears to be slight migration on the edges of the aggregates but nothing significant. Overall, the aggregates retained the proper shape while being stretched in the gel.

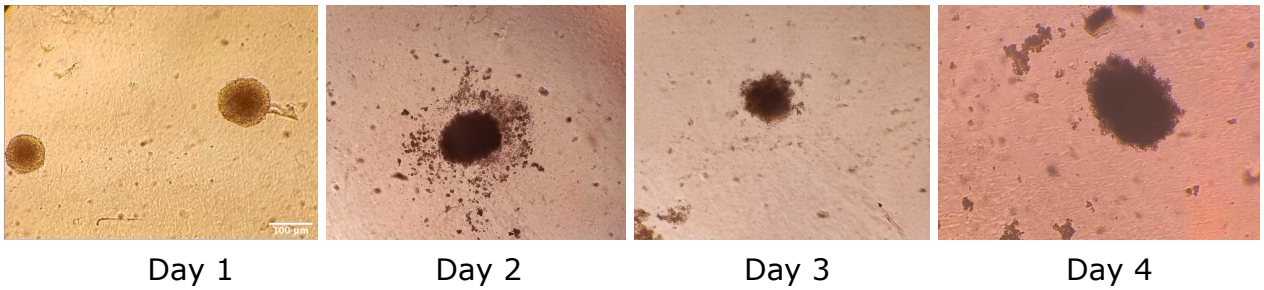

Figure 27: Fibrin Embedded Spheroids in CellScale (10x)

One day after embedding, the fibrin aggregates showed signs of migration. This continues throughout the remainder of the trial. The surrounding areas were covered with cell debris, but even on day 4 the migrated aggregate still managed to keep a relatively spherical shape.

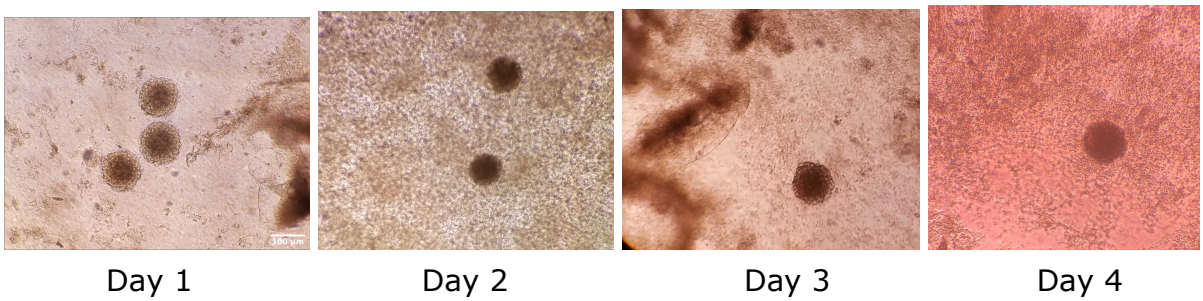

Figure 28: GelMA+HAMA Embedded Spheroids in CellScale (10x)

The GelMA+HAMA aggregates had strange debris floating around the fully formed aggregates. These could be cell debris, but a more likely possibility is that the GelMA+HAMA solution was not fully dissolved before embedding. It could also be a companiation of debris and the texture of the gel. Throughout the trial, the aggregates remained mostly spherical.

5.6 Stretching

Once the spheroids were embedded in the gels, they were mechanically stretched. This is done to mimic the environment in a heart valve when tensile stress is applied via transvalvular pressure. Uniaxial stretch was used for this process because the system is simpler to set up, use, and analyse; uniaxial is also better representative of the stresses applied to some vascular cells.

The best machine to meet the team's constraints is the CellScale MCFX (Figure 29). It is a high throughput uniaxial stimulation system of cell cultures. It is a 9x9x10 cm system with a cell monolayer configuration. The cell culture area is 16 wells (8x8mm), with a maximum strain of 12.5% and a maximum velocity of 10 mm/s. The maximum cycle frequency is 5 Hz and loading capacity is 30 N. This device meets the constraints the team had of 1-10% strain at 1 Hz.

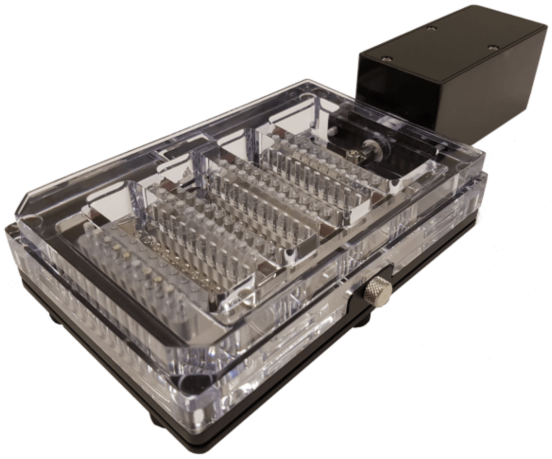

Figure 29: CellScale MCFX [Reported with approval, Zeugolis & Amsden, 2020]

The system uses flexible silicone well plates with "fingers" in them. These fingers will stick into the hydrogel in order to keep it in place. There was concern that the hydrogels would "pop" out of the plates because the "fingers" did not hold them well enough. In experimentation, the team found that the gels did not slip while using the 3mm plates. This was tested with fibrin, collagen, and GelMA+HAMA gels. These gels were tested at 10% stretch for 30 seconds, and a recovery of 30 seconds. These settings were enabled in the CellScale software and the menu setting summary chosen can be found in Appendix H.

Ideally, the gels will be stretched for 7 days. This would provide an accurate comparison between 2D and 3D systems, since similar experiments are being performed for 2D. This timeline would be dependent on the life of the cells. Based on research from Roosens et al., aggregates showed signs of calcification within 1 day, and were no longer viable after day 9. Edits to this method can be made based on how stretching slows or speeds up calcification. It will also be dependent on the "fingers" in the CellScale plate. Testing for a limited time, the gels did not pop out, but a longer time period stretching could affect this.

To complete the final design validation and initial step of data collection, the gels were imaged. The CellScale MCFX model does not have an imaging program built in, so a macro lens and a lightbox was used to image. This setup can be seen in figure 30 below. Each day, a few second video was taken and 10 images were extracted from it.

Figure 30: Experimental Setup

In order to verify the strain, a powder was spread onto the gels. This was done by filing down graphite and spreading it onto the gel. Initially, the graphite powder was spread onto the gel and then was set in the incubator for an hour. After incubation, the graphite in the collagen and fibrin settled in a different pattern than the initial spread. The fibrin graphite spread into a diagonal line, whereas the collagen graphite was clumped into the middle. This is shown in figure 31 below.

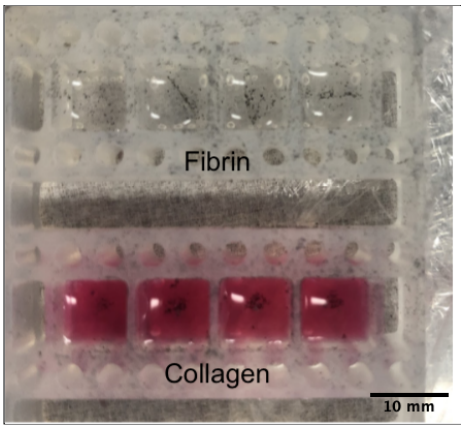

Figure 31: Graphite Pattern in Collagen and Fibrin

After this initial attempt, the graphite was later embedded in a similar fashion to the aggregates. The pre-polymer solution was created and then the graphite powder was placed in the solution. It was then mixed by pipetting up and down, then pipetted into the CellScale microwells. From here, the solution was incubated as appropriate. This strain pattern in a collagen gel can be seen in figure 32 below.

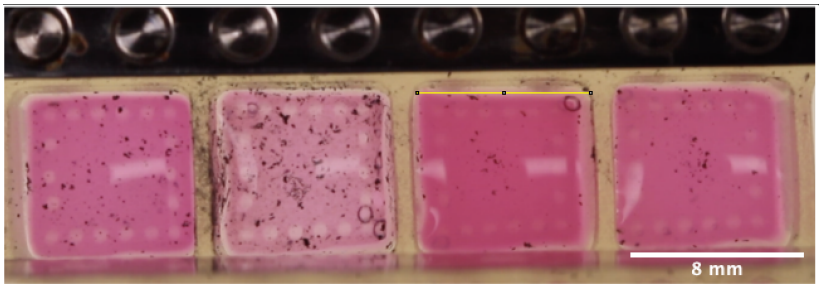

Figure 32: Graphite Pattern in Collagen Gel

From the images taken, they were put into a GUI particle image velocimetry software add-on inMatlab to analyze the strain distribution over the gel. This was done over the course of the seven days. However, in order to initially test that the CellScale was stretching 10%, the video from day 1 of stretching was inputted into ImageJ. A screenshot was taken of the gel stretching from its original point, to its final stretch peak before it continues back to its original position.

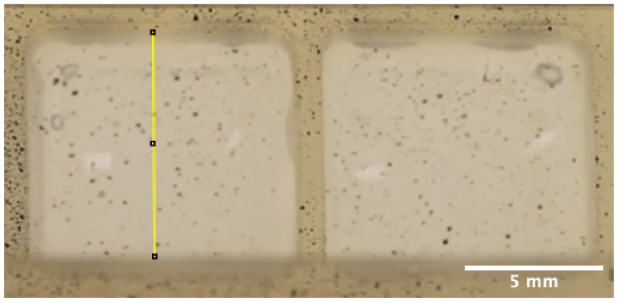

Figure 33a: Original length (8mm)

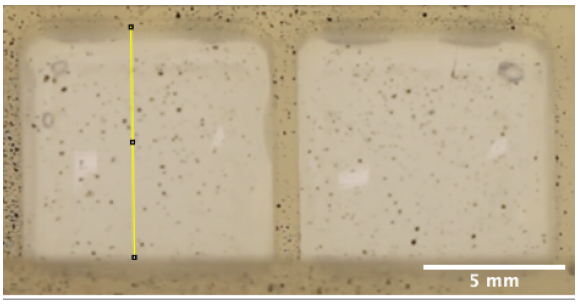

Figure 33b: Secondary length (8.775 mm)

Following equation 1, the data was inputted and the estimate of strain was calculated. Though this method is not completely accurate due to human error in selecting data points, the estimated 9.6% strain proves that the CellScale was being stretched approximately 10%.

$$\varepsilon = \frac{\Delta L}{L} \tag{1}$$

$$\varepsilon = \frac{\Delta L}{L} = \frac{0.775}{8} = 9.6\% \text{ strain}$$

Following embedding and stretching, the next steps were to complete the final design validation. This involves testing the cells were alive, showed signs of calcification, and were actually stretched at 10% strain over the course of the testing period.

Chapter 6: Final Design and Validation

Validation testing was needed to ensure that the client's specifications would be met. The following section explains how the design, including the gels, aggregates, and CellScale system were validated.

Since material property tests could not be conducted on the gels, verification was completed through imaging and staining. Imaging was completed daily on the microscope, and staining was conducted to ensure the embedded aggregates were alive and calcified. Standard staining of 3D constructs require paraffinization and sectioning to effectively expose the construct to the stains. However, a fellow researcher has successfully stained VIC aggregates without sectioning with a live/dead and calcification staining protocol, so the team was hopeful that it would also be possible for the stains to permeate the hydrogels, as they are presumed to be more permeable than the VIC spheroids.

6.1 Live Dead Staining

One day after embedding the aggregates into the static gels, a live/dead test was conducted to ensure the viability of the spheroids. The life stain is calcein, which permeates the cell membrane and stains part of the cytoplasm. If the cell is dead, the membrane will perforate and the cytoplasm will leak out. This causes weak results to the stain, showing no sign of stain fluorescence. The live cells will appear green during imaging. The dead stain is propidium iodide, which is impermeable to the cell membrane. Instead, it stains the DNA. If the cell is dead, the membrane will be perforated and the stain will reach the inside of the nucleus causing a light pattern. Dead cells appear red during imaging.

After staining aggregates in all three gels, the collagen appeared to have the best results. As seen in figure 34, there were mainly signs of live cells in every well plate. The fibrin, however, had begun to disaggregate and showed signs of some live cells with mainly dead around the edges, as seen in figure 35. The aggregates in the GelMA+HAMA cogel had less clear results. The live and dead stains were both similarly weak, so it is possible that the material properties of the gel prevented the stain from being successful. Originally, the team believed the 90 second UV exposure was too much and killed the cells. A second trial was conducted with 30 second UV exposure and the results were the same. Further images of the stained aggregates can be found in Appendix I.

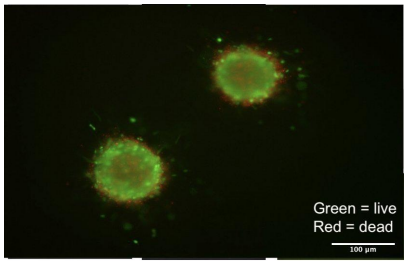

Figure 34: Collagen live dead

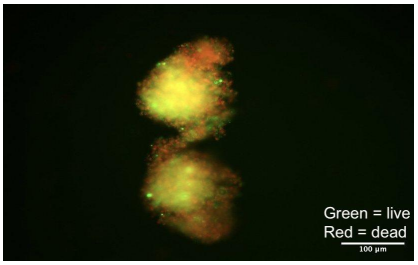

Figure 35: Fibrin live dead

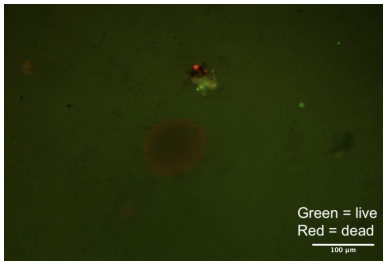

Figure 36: GelMA live dead

6.2 Von Kossa Calcification Staining

The Von Kossa staining protocol consisted of silver nitrate deposition and a nuclear counterstain (Appendix J). While the silver nitrate deposition is not limited to calcium (e.g. it will also occur with potassium), it was shown to be more effective in our lab than Alizarin Red. Calcium would appear grey or black, and the counterstain was Nuclear Fast Red. This was performed five days after embedding.

In contrast to the live/dead staining, the Von Kossa calcification stain had little success. The spheroids in fibrin were able to be imaged (Fig. 37), but no calcium deposits were detected with any certainty. The dark spotted background made it difficult to determine what was stained within the aggregate itself.

The silver nitrate was not able to be rinsed out of the other two gels. After UV exposure with silver nitrate, both collagen and GelMA+HAMA seemed to polymerize further, resulting in the ability to handle them (Fig. 38-39). The upper half of both gels became darkened to the point of being nearly impossible to image through.

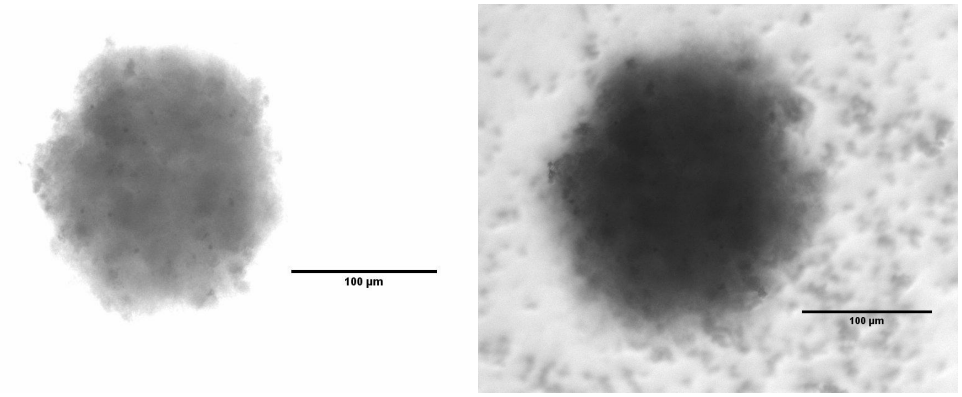

Figure 37: Fibrin Von Kossa Calcification Stain
Images are of the same aggregate with different exposures to demonstrate the ambiguity of the textured background.

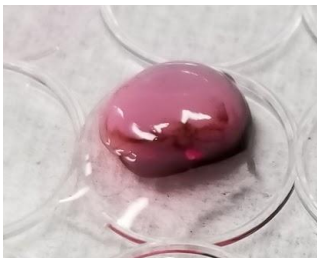

Figure 38: Collagen Gel, Inverted After Von Kossa Calcification Stain
Gel is inverted on the lid of a 96 well plate. The collagen gel is pink from the phenol red in the media, but now more opaque. A point of nuclear red is visible, as is the darkness caused by the silver nitrate solution.

Figure 39: GelMA+HAMA Gel, Side View After Von Kossa Calcification Stain
Gel is almost completely dark, though the underside (bottom left) is lighter and more red than the dark brown top side.

6.3 Strain Verification

In order to verify more accurately that the CellScale was stretching the gels at 10% strain, PIV Matlab was used. A 0.96 second video (1 cycle of stretch) of fibrin being stretched was uploaded into the program. The video was taken at 30.3 FPS. Multiplying the FPS by the video length gives the total amount of frames as shown in equation 2 below.

$$\text{Frames} = \frac{Frames}{second} * \text{time (s)} \qquad (2)$$

Based on this, the total amount of frames for the video was 29.088. This video was uploaded into PIV lab and data was extracted every frame. The first 15 frames show the initial stretch, and the second 14 show the gel going back to its original position.

The images were analyzed in pixels in order to remove the potential error of calibrating into mm. The arrows shown in the images below represent the strain rate vectors. The arrow placements are the same for each of the 29 frames. The pixels were analyzed at 128 pixels, then again at 64 px. This causes an 8 vector by 8 vector system. Figure 40 below shows the location in the well plate where each strain point is analyzed (marked by a green arrow).

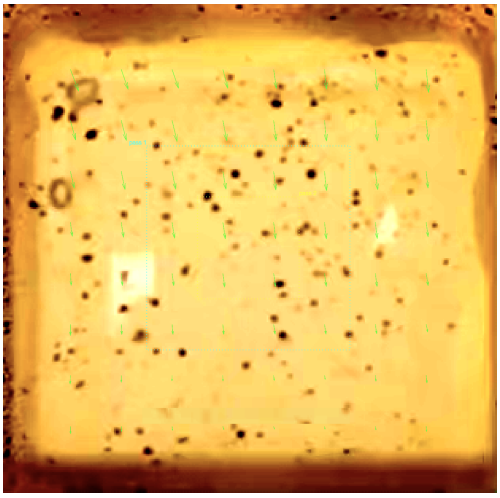

Figure 40: Vector placement in the well plate

From each point over the course of every frame, the strain rate was extracted. To convert from strain rate to strain, the total time per frame was calculated. The total video is 0.96 seconds and there are 29 frames, meaning the frame intervals are at 0.0331 seconds. The strain rates were multiplied by time, and the strains for each frame were summed together. Each vector was added until the frames started returning a negative strain. This negative gives indication that the gel began moving in the opposite direction. This occurred on frame 16, so frames 1-15 represent strain. This summation of strain was ~7.47%. To examine the process of calculation strain relative to displacement, see Appendix K.

Figure 41 below analyzes the strain in the y direction. The average strain over-all is approximately 7%. The bottom data may be skewed due to video quality or the angle the CellScale was filmed at. Similarly, the same process was completed for the x direction, which should be close to 0%, since there is no stretch in the x-axis for a biaxial system.

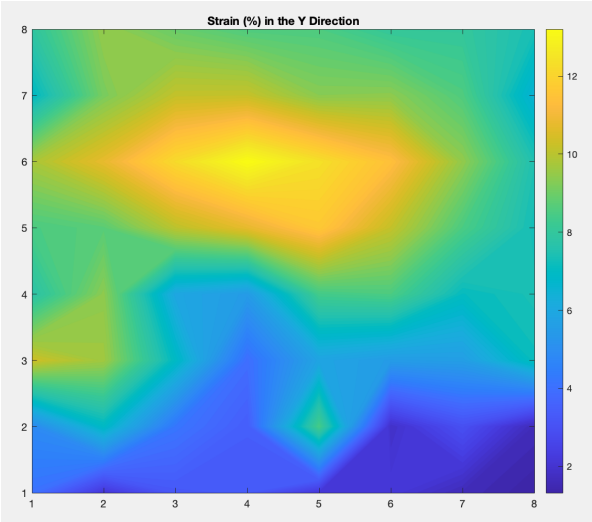

Figure 41: Strain of all 15 frames in the Y direction

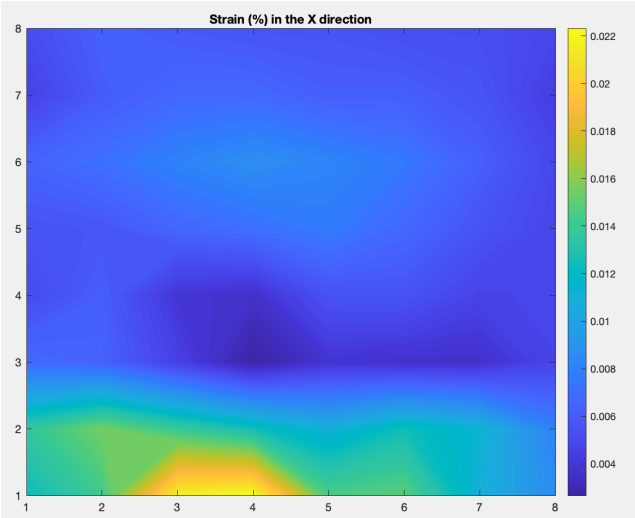

Figure 42: Strain of all 15 frames in the X direction

Chapter 7: Discussion

The main goal of this Major Qualifying Project was to develop a 3D *in vitro* model to study the mechanism of VIC dystrophic calcification. Currently, there are no effective models on the market that can model 3D calcification. After a final model was chosen, the testing done verified that almost all of the client's constraints were met. Table 13 below reiterates the constraints and marks whether or not they were met.

Table 13: Final Constraints

Objective	Constraints	Met?
Low cost	$1,000 total budget	✔
	< $500 for substrate materials	✔
Easy use	Does not involve advanced chemistry	✔
	Limited time per day commitment	✔
Rapid calcification	Lifetime of cells within the substrate	✔
Mechanically stresses cells	1-10% stretch at 1 Hz	✔
Models aortic valve stresses	Must be cyclic	✔
Models aortic valve biochemistry	Must use VICs	✔
Models aortic valve ECM	Similar stiffness to the valve	**?**
Models dystrophic calcification	Must calcify, preferably without osteogenic media	**?**

The aggregate creation method using the Agarose microwells was very successful. This design consistently produced viable aggregates. After a few unsuccessful trials, however, the team learned it is very important to the integrity of the system to autoclave both the molds and the aggregates before use to ensure optimal sterilization.

Two alternate methods were tested to embed aggregates - flipping the mold and mixing the aggregates directly with the pre-polymer solution, and individually pipetting the aggregates. While both were successful, the former was much easier and more effective than the latter. However, using a combination of both methods is the best choice. First, the mold should be flipped and mixed with the pre-polymer solution. After pipetting the gel into the wells, they should be taken to the microscope to ensure the

aggregates were properly embedded. If some wells did not get aggregates or have very few, then it is more effective at this point to individually pipette aggregates on top of the gel (before curing) .

While the initial assumption was that only one gel would be chosen for our application, further testing concluded that all three gels are beneficial in their own way. For this project specifically, it is recommended that collagen gel is used. In addition to the natural healing properties of the gel, it safely housed the spheroids in comparison to the other gels. While the gels did slightly migrate and connect to the fibers of the gel, they remained mostly intact. This method could also be suited well for models that need cell integration into the gel. This gel also had the most positive results in terms of cell viability. The live dead staining consistently showed signs of live cells. While our calcification stain was ineffective, paraffinization and sectioning would almost certainly provide high quality results, similar to that of staining native tissue.

The fibrin gel, though a similar material property to collagen, is not ideal for this application. Due to disaggregation in every trial conducted, this gel would be better suited if migration was desired. In addition to the cell migration, the embedded aggregates showed a higher percentage of dead cells than live, and had much less live cells than the collagen gel. Though there is promise for staining protocols without sectioning, this mild benefit is likely not worth consideration in comparison to the other features of this gel.

The GelMA+HAMA co-gel was, overall, also promising. If further testing was conducted, the viability of the gel could be better proven. The embedded spheroids showed no signs of movement or disaggregation over the testing period. However, the live dead stain led to inconclusive results - cell viability nor death was positively detected. This could be due to cell death from the UV exposure or material properties of the gel itself. Experimenting more with the UV exposure length and alternate stain types could provide more decisive results. Similar to collagen, sectioning is required to perform a calcification stain on this gel, as per laboratory standard.

In order to verify the CellScale stretch, graphite powder was spread onto the gels and imaged every day. The gel was preliminarily analyzed in ImageJ by comparing the original distance to the final distance. This strain was calculated to be approximately 9.6%. After this, a video of one cycle of stretch was analyzed in Matlab. The average strain for this fibrin verification was ~7.47%. Based on all the verification, the system is estimated to have accurately stretched the aggregates at ~10% strain.

Overall, the final model was simple and allowed for minimum time per day commitment. Since rheology could not be completed, the team could not completely verify the stiffness of the gels. Aside from this, and the calcification staining issues, all other constraints were met.

Chapter 8: Project Impact

8.1 Economic Considerations

A detailed breakdown of the cost of the materials used for this project can be found in Appendix A. The maximum cost for the device was $1000, in total the team spent $964. However, many of the items used were not considered in the final cost. In order to replicate this design, client's would need to purchase a CellScale MCFX, CellScale plates, Agarose, gel materials of choice, and the molds. To purchase the CellScale system and plates together, this would cost approximately $7,000. The gel, depending on which is chosen, would be around $200. The microwells, from Sigma Aldrich, are approximately $500. Not including the porcine VICs, the system would cost approximately $8,000 to replicate. Another uniaxial stretch system could be used if easily accessible.

8.2 Environmental Impact

Environmental factors must be considered when creating a novel model of disease. Through our development process, there was an effort to mitigate any potential negative effects that could arise with the production of our design. An area of concern that was identified was the use of the single-use silicone CellScale plates. There was an attempt to clean out the hydrogels from the wells in order to assess if the flexible plates could be sterilized again and reused, but the fingers in each well made this task extremely difficult. As a result, it was concluded that the plates could not be reused and had to be disposed appropriately. Future attempts to optimize this feature should be pursued.

8.3 Social Impact

When considering the social implications of a working model such as the one developed for this project, a focus on the purpose of it had to be emphasized. This model could in theory allow for future researchers to gain a better understanding of how the mechanism of VIC dystrophic calcification works and how it affects CAVD. In gaining more knowledge of the functioning, pathways, and mechanics of the disease, further efforts could be attempted so as to try to better prevent it and treat it in more efficient ways. This would allow for a great portion of the population currently being affected by CAVD to potentially obtain better care and enjoy a healthier life.

8.4 Ethical Considerations

The model proposed in this report is not a major source of ethical concern. Since one of the main purposes of this study is to further comprehend the mechanism of CAVD in order to develop a treatment that could potentially provide a permanent solution to the condition, the in vitro tests performed are justified. The only potential ethical concern would be the sourcing of the cell line used as it is derived from a porcine source. There have been various ethical debates regarding the use of animal derived tissues for human benefit as no unnecessary suffering should be caused to an animal. For this reason, reduction of the cell quantities used for this protocol could be put in place by refining the methods to minimize waste

and eventually, replacement of the cell lines used could also be a possibility if sourcing from human specimens is feasible. Furthermore, the potential outcomes derived from the data obtained through this model could aid in redirecting the focus of CAVD treatment from using porcine valves to a potential cure, eliminating the extended use of animal models.

8.5 Public Health, Safety, and Welfare

The model does not pose any public health or safety concern to either the user of this model. The best way to protect the health and safety of the user is for the user to practice excellent lab safety protocols and wear personal protective equipment. Such will ensure that the patient does not get any fluids in the eyes nor on the skin, protecting the user from any bodily reactions to the fluids used.

The model will positively impact the health, safety and welfare of human lives by allowing for a better understanding of the mechanism of CAVD, to assist in creating a treatment for CAVD in patients. Such will allow the patients to live an optimal, healthier life.

Chapter 9: Conclusions & Recommendations

9.1 Conclusion

The main goal of this Major Qualifying Project was to develop a 3D *in-vitro* model to study the mechanism of VIC dystrophic calcification. The final design verification has shown this goal was accomplished. The system could function using three potential gels, collagen, fibrin, and GelMA+HAMA. The final recommendation for this system is to use the collagen gel. Using the agarose mold method, functional aggregates were created most times. One day after embedding aggregates into the collagen gels, the live dead stain showed consistent signs of live cells. On day 5 after embedding, the fibrin aggregates showed signs of calcification, however the other gels did not. Based on earlier research conducted in the Billiar lab on aggregates that are not embedded, the team is confident that there was calcification and the stain did not work properly. The stretching capability was verified in Matlab and ImageJ to operate at 10% strain.

9.2 Future Recommendations

The final device met the client's requirements for the project, but improvements to increase functionality can still be made. The gel properties can be tuned better to fit specific research interest —for each gel, we followed protocols that we had known to be effective, but there is a range of concentrations of the polymer. More testing would also provide more reliable and robust data for future researchers to work off of; while all of the gels chosen show promise and mostly consistent results, the limited number of trials reduces statistical confidence. Further work also enables other aspects to be characterized, particularly through rheological testing and the use of other stains.

The live/dead staining protocols for the GelMA+HAMA co-gel could also be better refined. The staining results across the three gels were inconsistent, so further research into alternate staining protocols would be beneficial. The Von Kossa Calcification staining protocols could also be better adjusted. Since non-embedded aggregate work in Billiar's lab showed calcification, the embedded aggregates should have shown signs, as well. Researching more effective stains for each gel could better validate the data the team gathered.

References

Antoni, D., Burckel, H., Noel, G., & Josset, E. (2015). Three-Dimensional Cell Culture: A Breakthrough in Vivo. *International Journal of Medical Sciences, 16*(3), 5517-5527. doi:10.3390/ijms16035517

Assmann, A., Vegh, A., Ghasemi-Rad, M., Bagherifard, S., Cheng, G., Sani, E. S., & Annabi, N. (2017). A highly adhesive and naturally derived sealant. *Biomaterials, 140*, 115-127. doi:10.1016/j.biomaterials.2017.06.004

Balachandran, K., Sucosky, P., & Yoganathan, A. P. (2011). Hemodynamics and mechanobiology of aortic valve inflammation and calcification. *International journal of inflammation*, 2011.

Balachandran, K., Sucosky, P., Jo, H., & Yoganathan, A. P. (2009). Elevated cyclic stretch alters matrix remodeling in aortic valve cusps: implications for degenerative aortic valve disease. American *Journal of Physiology-Heart and Circulatory Physiology*, 296(3), H756-H764.

Bell, B., Nauman, E., & Voytik-Harbin, S. (2012). Multiscale strain analysis of Tissue Equivalents using a Custom-Designed biaxial testing device. *Biophysical Journal, 102*(6), 1303-1312. doi:10.1016/j.bpj.2012.02.007

Benton, J.A., Fairbanks, B. D., & Anseth, K. S. (2009). Characterization of valvular interstitial cell function in three dimensional matrix metalloproteinase degradable PEG hydrogels. *Biomaterials, 30*(34), 6593-6603. doi:10.1016/j.biomaterials.2009.08.031

Bierbaum, S., Hintze, V., & Scharnweber, D. (2017). 2.8 Artificial Extracellular Matrices to Functionalize Biomaterial Surfaces. *Comprehensive Biomaterials II,* 131-132. doi:10.1016/b978-0-12-803581-8.10206-1

Boudou, T., Ohayon, J., Picart, C., Pettigrew, R. I., & Tracqui, P. (2009). Nonlinear elastic properties of polyacrylamide gels: implications for quantification of cellular forces. Biorheology, 46(3), 191-205.

Bowler, M. A., & Merryman, W. D. (2015). In vitro models of aortic valve calcification: Solidifying a system. *Cardiovascular Pathology, 24*(1), 1-10. doi:10.1016/j.carpath.2014.08.003

Bresciani, G., Hofland, L. J., Dogan, F., Giamas, G., Gagliano, T., & Zatelli, M. C. (2019). Evaluation of Spheroid 3D Culture Methods to Study a Pancreatic Neuroendocrine Neoplasm Cell Line. *Frontiers in Endocrinology, 10*. doi:10.3389/fendo.2019.0068

Breslin, S. & O'Driscoll, L. (2013). Three-dimensional cell culture: The missing link in drug discovery. Drug Discovery Today, 18(5-6), 240-249. doi:10.1016/j.drudis.2012.10.003

Brown, T. D. (2000). Techniques for mechanical stimulation of cells in-vitro: a review. *Journal of biomechanics*, 33(1), 3-14.

Caliari, S. R., & Burdick, J. A. (2016). A practical guide to hydrogels for cell culture. *Nature Methods, 13*(5), 405-414. doi:10.1038/nmeth.3839

Camci-Unal, G., Cuttica, D., Annabi, N., Demarchi, D., & Khademhosseini, A. (2013). Synthesis and characterization of hybrid hyaluronic acid-gelatin hydrogels. Biomacromolecules, 14(4), 1085-1092.

Charoen, K., Fallica B., Colson, Y., Zaman, H., & Grinstaff, M. (2014). Embedded multicellular spheroids as a biomimetic 3D cancer model for evaluating drug and drug-device combinations, *Biomaterials, 35(7),* 2264-2271. doi:10.1016/j.biomaterials.2013.11.038.

Chen, H. Y., Engert, J. C., & Thanassoulis, G. (2019). Risk factors for valvular calcification. *Current opinion in endocrinology, diabetes, and obesity*, 26(2), 96.

Davis, C. A., Zambrano, S., Anumolu, P., Allen, A. C., Sonoqui, L., & Moreno, M. R. (2015). Device-based in vitro techniques for mechanical stimulation of vascular cells: A review. *Journal of Biomechanical Engineering, 137*(4). doi:10.1115/1.4029016

Duchi, S., Onofrillo, C., O'Connell, C. D., Blanchard, R., Augustine, C., Quigley, A. F., Choong, P. F. (2017). Handheld Co-Axial Bioprinting: Application to in situ surgical cartilage repair. *Scientific Reports, 7*(1). doi:10.1038/s41598-017-05699-x

Duval, K., Grover, H., Han, L., Mou, Y., Pegoraro, A. F., Fredberg, J., & Chen, Z. (2017). Modeling Physiological Events in 2D vs. 3D Cell Culture. *Physiology, 32*(4), 266-277. doi:10.1152/physiol.00036.2016

Edmondson, R., Broglie, J. J., Adcock, A. F., & Yang, L. (2014). Three-Dimensional Cell Culture Systems and Their Applications in Drug Discovery and Cell-Based Biosensors. *ASSAY and Drug Development Technologies, 12*(4), 207-218. doi:10.1089/adt.2014.573

Fairbanks, B. D., Schwartz, M. P., Halevi, A. E., Nuttelman, C. R., Bowman, C. N., & Anseth, K. S. (2009). A Versatile Synthetic Extracellular Matrix Mimic via Thiol-Norbornene Photopolymerization. *Advanced Materials, 21*(48), 5005-5010. doi:10.1002/adma.200901808

FDA. (2020, September 4). *Use of International Standard ISO 10993-1, "Biological evaluation of medical devices - Part 1: Evaluation and testing within a risk management process"*. Guidance for Industry and Food and Drug Administration Staff.

Freeman, R. V., & Otto, C. M. (2005). Spectrum of Calcific Aortic Valve Disease. *Circulation, 111*(24), 3316-3326. doi:10.1161/circulationaha.104.486738

Gilbert, S. F. (2000). Osteogenesis: The Development of Bones. In S. F. Gilbert, S. R. Singer, M. S. Tyler, & R. N. Kozlowski (Authors), *Developmental Biology* (6th ed., pp. 170-176). Sunderland, MA: Sinauer Associates. Retrieved November 23, 2020, from https://www.ncbi.nlm.nih.gov/books/NBK10056/

Grinnell, F. (2003). Fibroblast biology in three-dimensional collagen matrices. *Trends in Cell Biology, 13*(5), 264-269. doi:10.1016/s0962-8924(03)00057-6

Han, C., Takayama, S., & Park, J. (2015). Formation and manipulation of cell spheroids using a density adjusted PEG/DEX aqueous two phase system. Scientific reports, 5, 11891.

Hasan, A., Ragaert, K., Swieszkowski, W., Selimović, Š, Paul, A., Camci-Unal, G., . . . Khademhosseini, A. (2014). Biomechanical properties of native and tissue engineered heart valve constructs. *Journal of Biomechanics, 47*(9), 1949-1963. doi:10.1016/j.jbiomech.2013.09.023

Hjortnaes, J., Goettsch, C., Hutcheson, J. D., Camci-Unal, G., Lax, L., Scherer, K., . . . Aikawa, E. (2016). Simulation of early calcific aortic valve disease in a 3D platform: A role for myofibroblast differentiation. *Journal of Molecular and Cellular Cardiology, 94*, 13-20. doi:10.1016/j.yjmcc.2016.03.004

Hjortnaes, J., Goettsch, C., Hutcheson, J. D., Camci-Unal, G., Lax, L., Scherer, K., . . . Aikawa, E. (2014). Directing valvular interstitial cell myofibroblast-like differentiation in a hybrid hydrogel platform. *Advanced Healthcare Matterials, 4(1),* 121-130. doi: 10.1002/adhm.201400029.

Hsu, J. J., Lim, J., Tintut, Y., & Demer, L. L. (2016). Cell-matrix mechanics and pattern formation in inflammatory cardiovascular calcification. *Heart, 102*(21), 1710-1715. doi:10.1136/heartjnl-2016-309667

Huh, D., Hamilton, G. A., & Ingber, D. E. (2011). From 3D cell culture to organs-on-chips. *Trends in cell biology*, 21(12), 745-754.

Im Cho, K., Sakuma, I., Sohn, I. S., Jo, S. H., & Koh, K. K. (2018). Inflammatory and metabolic mechanisms underlying the calcific aortic valve disease. *Atherosclerosis*, 277, 60-65.

Kural, M. H., & Billiar, K. L. (2013). Regulating tension in three-dimensional culture environments. *Experimental Cell Research, 319*(16), 2447-2459. doi:10.1016/j.yexcr.2013.06.019

Kurpinski, K., Park, J., Thakar, R., & Li, S. (2006). Regulation of Vascular Smooth Muscle Cells and Mesenchymal Stem Cells by Mechanical Strain. *Molecular & Cellular Biomechanics, 3*(1), 21-34. doi:10.3970/mcb.2006.003.021

Leopold, J. (2012, August 1). Cellular mechanisms of aortic valve calcification. Retrieved October 05, 2020, from https://www.ncbi.nlm.nih.gov/pmc/articles/PMC3427002/

Lerman, D. A., Prasad, S., & Alotti, N. (2015, October 28). Calcific Aortic Valve Disease: Molecular Mechanisms And Therapeutic Approaches. *European Cardiology Review, 10*(2). doi:https://doi.org/10.15420/ecr.2015.10.2.108

Li, Y., Meng, H., Liu, Y., & Lee, B. P. (2015). Fibrin Gel as an Injectable Biodegradable Scaffold and Cell Carrier for Tissue Engineering. *The Scientific World Journal, 2015*, 1-10. doi:10.1155/2015/685690

Lim, J., Ehsanipour, A., Hsu, J. J., Lu, J., Pedego, T., Wu, A., . . . Tintut, Y. (2016). Inflammation Drives Retraction, Stiffening, and Nodule Formation via Cytoskeletal Machinery in a Three-Dimensional Culture Model of Aortic Stenosis. *The American Journal of Pathology, 186*(9), 2378-2389. doi:10.1016/j.ajpath.2016.05.003

Litvinov, L., & Weisel, J. (2017). Fibrin mechanical properties and their structural origins. *Matrix Biology, 60*, 110-123. doi:10.1016/j.matbio.2016.08.003

Mabry, K. M., Payne, S. Z., & Anseth, K. S. (2016). Microarray analyses to quantify advantages of 2D and 3D hydrogel culture systems in maintaining the native valvular interstitial cell phenotype. *Biomaterials, 74*, 31-41. doi:10.1016/j.biomaterials.2015.09.035

Maritan, S. M., Lian, E. Y., & Mulligan, L. M. (2017). An Efficient and Flexible Cell Aggregation Method for 3D Spheroid Production. *Journal of Visualized Experiments,* (121). doi:10.3791/55544

Masters, K. S., Shah, D. N., Walker, G., Leinwand, L. A., & Anseth, K. S. (2004). Designing scaffolds for valvular interstitial cells: Cell adhesion and function on naturally derived materials. *Journal of Biomedical Materials Research, 71A*(1), 172-180. doi:10.1002/jbm.a.30149

Mirab, F., Kang, Y. J., & Majd, S. (2019). Preparation and characterization of size-controlled glioma spheroids using agarose hydrogel microwells. *Plos One, 14*(1). doi:10.1371/journal.pone.0211078

Mohler III, E. R., Gannon, F., Reynolds, C., Zimmerman, R., Keane, M. G., & Kaplan, F. S. (2001). Bone formation and inflammation in cardiac valves. Circulation, 103(11), 1522-1528.

Montesano, R., & Orci, L. (1988). Transforming growth factor beta stimulates collagen-matrix contraction by fibroblasts: Implications for wound healing. *Proceedings of the National Academy of Sciences, 85*(13), 4894-4897. doi:10.1073/pnas.85.13.4894

Montorzi, G., Silacci, P., Zulliger, M., & Stergiopulos, N. (2004). Functional, mechanical and geometrical adaptation of the arterial wall of a non-axisymmetric artery in vitro. *Journal of Hypertension, 22*(2), 339-347. doi:10.1097/00004872-200402000-00018

Otto, C. M. (2008). Calcific Aortic Stenosis — Time to Look More Closely at the Valve. *New England Journal of Medicine, 359*(13), 1395-1398. doi:10.1056/nejme0807001

Otto, C. M., Kuusisto, J., Reichenbach, D. D., Gown, A. M., & O'brien, K. D. (1994). Characterization of the early lesion of 'degenerative' valvular aortic stenosis. Histological and immunohistochemical studies. *Circulation, 90*(2), 844-853. doi:10.1161/01.cir.90.2.844

Pick, A. (2019, February 27). Biocore Aortic Valve From St. Jude Medical. Retrieved October 05, 2020, fromhttps://www.heart-valve-surgery.com/heart-surgery-blog/2007/12/19/biocore-aortic-valve-from-st-jude-medical

Rajamannan, N. M., Evans, F. J., Aikawa, E., Grande-Allen, K. J., Demer, L. L., Heistad, D. D., . . . Otto, C. M. (2011). Calcific Aortic Valve Disease: Not Simply a Degenerative Process. *Circulation, 124*(16), 1783-1791. doi:10.1161/circulationaha.110.006767

Rodriguez, K. J., & Masters, K. S. (2009). Regulation of valvular interstitial cell calcification by components of the extracellular matrix. *Journal of Biomedical Materials Research Part A, 90A*(4), 1043-1053. doi:10.1002/jbm.a.32187

Roosens, A., Puype, I., & Cornelissen, R. (2017). Scaffold-free high throughput generation of quiescent valvular microtissues. *Journal of Molecular and Cellular Cardiology, 106*, 45-54. doi:10.1016/j.yjmcc.2017.03.004

Ruiz, J. L., Hutcheson, J. D., & Aikawa, E. (2015). Cardiovascular calcification: current controversies and novel concepts. Cardiovascular Pathology, 24(4), 207-212.

Rutkovskiy, A., Malashicheva, A., Sullivan, G., Bogdanova, M., Kostareva, A., Stensløkken, K., . . . Vaage, J. (2017, September 14). Valve Interstitial Cells: The Key to Understanding the Pathophysiology of Heart Valve Calcification. *Journal of the American Heart Association, 6*(9). doi:10.1161/jaha.117.006339

Ryu, N., Lee, S., & Park, H. (2019). Spheroid Culture System Methods and Applications for Mesenchymal Stem Cells. *Cells, 8*(12), 1620. doi:10.3390/cells8121620

Shah, N., Morsi, Y., & Manasseh, R. (2014). From mechanical stimulation to biological pathways in the regulation of stem cell fate. *Cell biochemistry and function*, 32(4), 309-325.

Shield, K., Ackland, M. L., Ahmed, N., & Rice, G. E. (2009). Multicellular spheroids in ovarian cancer metastases: Biology and pathology. *Gynecologic Oncology, 113*(1), 143-148. doi:10.1016/j.ygyno.2008.11.032

Sider, K. L., Blaser, M. C., & Simmons, C. A. (2011). Animal Models of Calcific Aortic Valve Disease. *International Journal of Inflammation,* 1-18. doi:10.4061/2011/364310

Soares, C., Midlej, V., Oliveira, M., Benchimol, M., Costa, M., & Mermelstein, C. (n.d.). 2D and 3D-Organized Cardiac Cells Shows Differences in Cellular Morphology, Adhesion Junctions, Presence of Myofibrils and Protein Expression. Retrieved December 11, 2020, from https://journals.plos.org/plosone/article?id=10.1371%2Fjournal.pone.0038147

Standards. ISO. (2021, February 19). https://www.iso.org/standards.html.

Standards by ISO/TC 276 . ISO. (2021, May 4). https://www.iso.org/committee/4514241/x/catalogue/.

Travis, B. R., Fowler, B. L., & Robicsek, F. (2009). A method for the measurement of left ventricular overload for aortic valve insufficiency. *Journal of biomechanics*, 42(12), 1935-1940.

Tsang, H. G., Cui, L., Farquharson, C., Corcoran, B. M., Summers, K. M., & Macrae, V. E. (2018). Exploiting novel valve interstitial cell lines to study calcific aortic valve disease. *Molecular medicine reports*, 17(2), 2100-2106.

Tuchin, V. (2015). Optical Properties of Tissues with Strong (Multiple) Scattering. In *Tissue optics: light scattering methods and instruments for medical diagnosis* (pp. 170–176). SPIE Press. https://doi.org/https://doi.org/10.1117/3.684093.ch1

Vdkerkhof, T. (2011). Triton™ Bi-Leaflet Prosthetic Heart Valve Aortic. Retrieved December 07, 2020, from http://comedbv.com/

Vyavahare, N. (2018). Bioprosthetic Heart Valves: From a Biomaterials Perspective. In 1111139329 839908644 H. Tam (Ed.), *Advances in Heart Valve Biomechanics* (pp. 337-382). Cham, Switzerland: Springer. Retrieved December 7, 2020, from https://doi.org/10.1007/978-3-030-01993-8

Wang, H., Haeger, S. M., Kloxin, A. M., Leinwand, L. A., & Anseth, K. S. (2012). Redirecting Valvular Myofibroblasts into Dormant Fibroblasts through Light-mediated Reduction in Substrate Modulus. *PLoS ONE, 7*(7). doi:10.1371/journal.pone.0039969

Weymann, Alexander. (2012). Reendothelialization of Human Heart Valve Neoscaffolds Using Umbilical Cord Derived Endothelial Cells. *Circulation Journal.*

Wilber, J. (2020, June 17). *What Exactly is ISO Certified? And Why Does it Matter?* Mead Metals, Inc. https://www.meadmetals.com/blog/what-exactly-is-iso-certified-and-what-does-it-mean.

Wipff, P., & Hinz, B. (2008). Integrins and the activation of latent transforming growth factor β1 – An intimate relationship. *European Journal of Cell Biology, 87*(8-9), 601-615. doi:10.1016/j.ejcb.2008.01.012

Wu, Y., Xiang, Y., Fang, J., Li, X., Lin, Z., Dai, G., Jin Y., Wei, P., Zhang, D. (2019). The influence of the stiffness of GelMA substrate on the outgrowth of PC12 cells. *Bioscience Reports*, *39*(1). https://doi.org/https://doi.org/10.1042/BSR20181748

Xing, Y., Warnock, J. N., He, Z., Hilbert, S. L., & Yoganathan, A. P. (2004). Cyclic pressure affects the biological properties of porcine aortic valve leaflets in a magnitude and frequency dependent manner. *Annals of biomedical engineering*, 32(11), 1461-1470.

Yamada, K., & Cukierman, E. (2007, August 23). Modeling Tissue Morphogenesis and Cancer in 3D.Retrieved December 11, 2020, from https://www.sciencedirect.com/science/article/pii/S0092867407010288

Yip, C. Y., Chen, J., Zhao, R., & Simmons, C. A. (2009). Calcification by Valve Interstitial Cells Is Regulated by the Stiffness of the Extracellular Matrix. *Arteriosclerosis, Thrombosis, and Vascular Biology, 29*(6), 936-942. doi:10.1161/atvbaha.108.182394

Yutzey, K. E., Demer, L. L., Body, S. C., Huggins, G. S., Towler, D. A., Giachelli, C. M., . . . Aikawa, E. (2014, September 4). Calcific Aortic Valve Disease. *Arteriosclerosis, Thrombosis, and Vascular Biology, 34*(11), 2387-2393. doi:10.1161/atvbaha.114.302523

Zeugolis, P., & Amsden, P. (n.d.). MCFX. Retrieved December 11, 2020, from https://www.cellscale.com/products/mcfx/

Zhang, X., Xu, B., Puperi, D. S., Wu, Y., West, J. L., & Grande-Allen, K. J. (2015). Application of Hydrogels in Heart Valve Tissue Engineering. *Journal of Long-Term Effects of Medical Implants, 25*(1-2), 105-134. doi:10.1615/jlongtermeffmedimplants.2015011817

Zuppinger, C. (2019). 3D cardiac cell culture: a critical review of current technologies and applications. *Frontiers in Cardiovascular Medicine*, 6, 87.

Appendix A: Cost and Budget Table

MQP Teams are allotted $250 per team member, resulting in a budget of $1000 for our team.

Item	Details	Price	Budget
Substrate Materials			~$500
GelMA w/ Irgacure		$135	
HAMA		$214	
Collagen		In lab	
Fibrinogen		In lab	
Thrombin	50 units	In lab, $95	
Other			~$500
CellScale plates (8)	With posts	$320	
Lab fee	$50 per team member	$200	
Total		**$964**	**$1000**

Appendix B: Figure Copyright Approval

Figure Description	Approval Statues	Documentation Uploaded
Figure 1: Aortic valve leaflet anatomy	Emailed - waiting for approval	
Figure 2: The progression of CAVD	No copyright approval needed for use in a thesis/ dissertation	Yes, tagline was used following the image
Figure 3: Mechanical valve	Emailed - waiting for approval	
Figure 4: Bioprosthetic valve	Approved	Yes
Figure 5: Scaffold-free aggregation methods a) pellet culture, b) liquid overlay, c) hanging drop, d) spinner culture, e) rotating wall vessel, f) microfluidics, g) magnetic levitation	Creative Common CC BY license	
Figure 6: Schematic diagrams of the traditional 2D monolayer cell culture (A) and 3D cell culture systems: cell spheroids/aggregates grown on matrix (B), cells embedded within matrix (C), and scaffold-free cell spheroids in suspension (D)	No copyright approval needed for use in a thesis/ dissertation	Yes
Figure 8: Design concept: aortic valve in left heart simulator.	Not copyrighted for non-commercial use	Yes
Figure 10: Cyclic pressure chamber.	Approved	Yes
Figure 13: Hanging Drop Method	Approved	Yes
Figure 14: ULA + MC	Not copyrighted for non-commercial use	Yes
Figure 15: Agarose microfabricated wells	Not copyrighted	Yes
Figure 16: MCFX CellScale plate	Emailed - waiting for approval	

Figure 23: CellScale MCFX	Emailed - waiting for approval	

Figure 2 Approval:

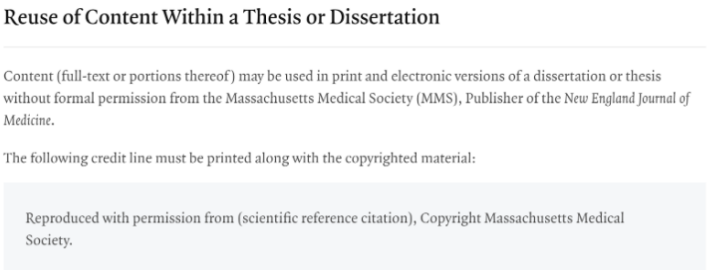

Reuse of Content Within a Thesis or Dissertation

Content (full-text or portions thereof) may be used in print and electronic versions of a dissertation or thesis without formal permission from the Massachusetts Medical Society (MMS), Publisher of the *New England Journal of Medicine*.

The following credit line must be printed along with the copyrighted material:

Reproduced with permission from (scientific reference citation), Copyright Massachusetts Medical Society.

Figure 4 Approval:

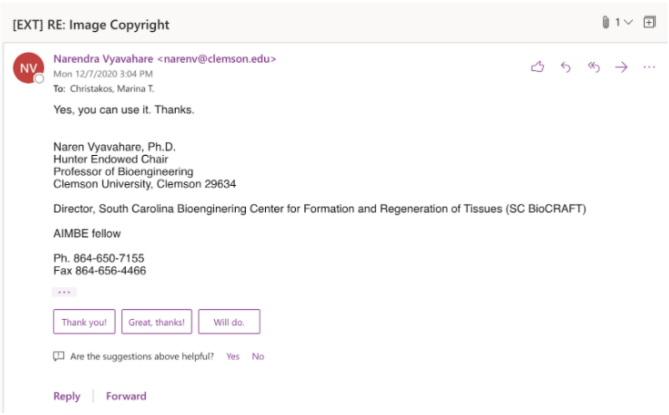

[EXT] RE: Image Copyright

Narendra Vyavahare <narenv@clemson.edu>
Mon 12/7/2020 3:04 PM
To: Christakos, Marina T.

Yes, you can use it. Thanks.

Naren Vyavahare, Ph.D.
Hunter Endowed Chair
Professor of Bioengineering
Clemson University, Clemson 29634

Director, South Carolina Bioenginering Center for Formation and Regeneration of Tissues (SC BioCRAFT)

AIMBE fellow

Ph. 864-650-7155
Fax 864-656-4466

Thank you! Great, thanks! Will do.

Are the suggestions above helpful? Yes No

Reply Forward

Figure 5 Approval:

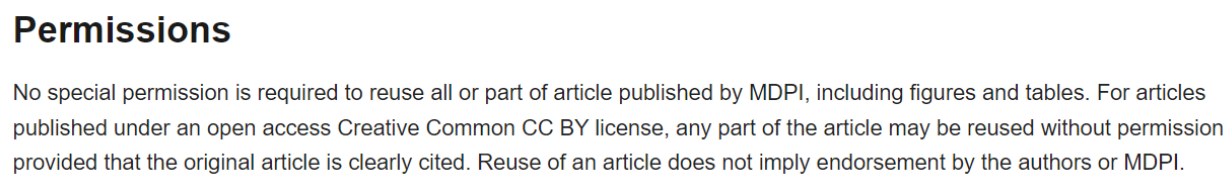

Permissions

No special permission is required to reuse all or part of article published by MDPI, including figures and tables. For articles published under an open access Creative Common CC BY license, any part of the article may be reused without permission provided that the original article is clearly cited. Reuse of an article does not imply endorsement by the authors or MDPI.

Figure 6 Approval:

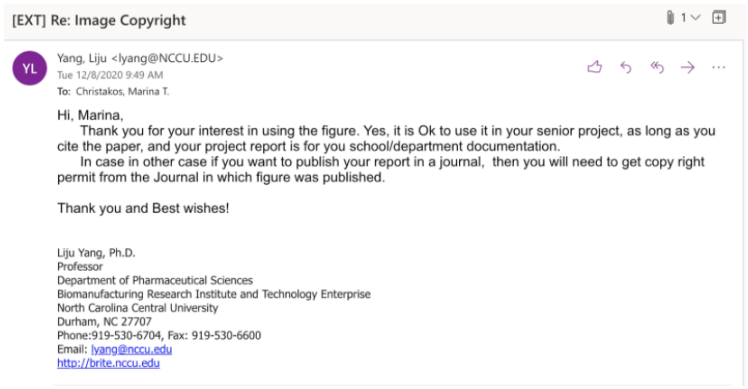

[EXT] Re: Image Copyright

Yang, Liju <lyang@NCCU.EDU>
Tue 12/8/2020 9:49 AM
To: Christakos, Marina T.

Hi, Marina,
Thank you for your interest in using the figure. Yes, it is Ok to use it in your senior project, as long as you cite the paper, and your project report is for you school/department documentation.
In case in other case if you want to publish your report in a journal, then you will need to get copy right permit from the Journal in which figure was published.

Thank you and Best wishes!

Liju Yang, Ph.D.
Professor
Department of Pharmaceutical Sciences
Biomanufacturing Research Institute and Technology Enterprise
North Carolina Central University
Durham, NC 27707
Phone:919-530-6704, Fax: 919-530-6600
Email: lyang@nccu.edu
http://brite.nccu.edu

Figure 7 Approval:

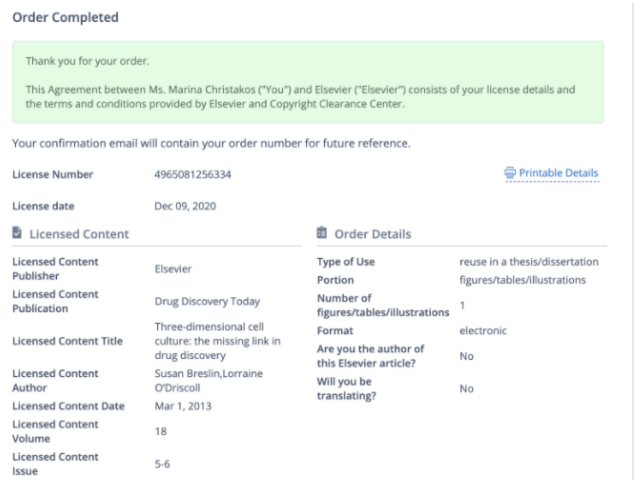

Order Completed

Thank you for your order.

This Agreement between Ms. Marina Christakos ("You") and Elsevier ("Elsevier") consists of your license details and the terms and conditions provided by Elsevier and Copyright Clearance Center.

Your confirmation email will contain your order number for future reference.

License Number	4965081256334
License date	Dec 09, 2020

Printable Details

Licensed Content

Licensed Content Publisher	Elsevier
Licensed Content Publication	Drug Discovery Today
Licensed Content Title	Three-dimensional cell culture: the missing link in drug discovery
Licensed Content Author	Susan Breslin,Lorraine O'Driscoll
Licensed Content Date	Mar 1, 2013
Licensed Content Volume	18
Licensed Content Issue	5-6

Order Details

Type of Use	reuse in a thesis/dissertation
Portion	figures/tables/illustrations
Number of figures/tables/illustrations	1
Format	electronic
Are you the author of this Elsevier article?	No
Will you be translating?	No

Figure 8 Approval:

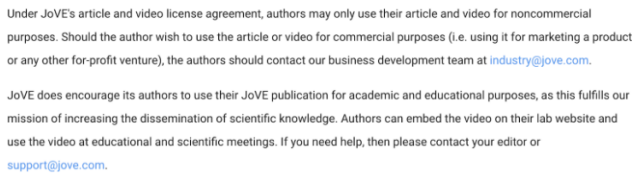

Under JoVE's article and video license agreement, authors may only use their article and video for noncommercial purposes. Should the author wish to use the article or video for commercial purposes (i.e. using it for marketing a product or any other for-profit venture), the authors should contact our business development team at industry@jove.com.

JoVE does encourage its authors to use their JoVE publication for academic and educational purposes, as this fulfills our mission of increasing the dissemination of scientific knowledge. Authors can embed the video on their lab website and use the video at educational and scientific meetings. If you need help, then please contact your editor or support@jove.com.

Figure 9 Approval:

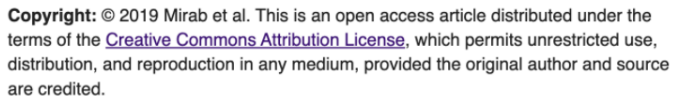

Copyright: © 2019 Mirab et al. This is an open access article distributed under the terms of the Creative Commons Attribution License, which permits unrestricted use, distribution, and reproduction in any medium, provided the original author and source are credited.

Figure 10 Approval:

This Agreement between Beck Arruda ("You") and Springer Nature ("Springer Nature") consists of your license details and the terms and conditions provided by Springer Nature and Copyright Clearance Center.

License Number 5062580847588

Order Details

Type of Use	Thesis/Dissertation
Requestor type	academic/university or research institute
Format	electronic
Portion	figures/tables/illustrations
Number of figures/tables/illustrations	1

Appendix C: Pairwise Comparisons

Within each objective, pairwise comparisons were completed to judge the importance of individual specifications. In Table A, the team created a pairwise analysis with our client in which aspects of the spheroid formation methods were assessed to determine which were the most important. The most important aspect is that aggregates of consistent sizes can be created, closely followed by the ability of creating a wide range of sizes. These were followed by having a high throughput, ease of process and short formation time, having a relatively low cost and finally, that no other chemicals were needed for the formation of these aggregates.

Table A: Spheroid Specifications Pairwise Comparison

	Creates consistent sizes	Range of sizes possible	No additional chemicals	Short formation time	Low cost	Ease of process	High throughput	Total	
Creates consistent sizes		1, 0, 1	1, 1, 1	1, 1, 1	1, 1, 1	1, 1, 1	1, 0, 1	5.33	5
Range of sizes possible	0, 1, 0		1, 1, 1	1, 1, 1	1, 1, 1	1, 1, 1	1, 0, 1	5.00	4
No additional chemicals	0, 0, 0	0, 0, 0		0, 0, 0	0, 0, 0	0, 0, 0	0, 0, 0	0.00	0
Short formation time	0, 0, 0	0, 0, 0	1, 1, 1		1, 1, 1	0, 1, 1	0, 0, 0	2.67	2
Low cost	0, 0, 0	0, 0, 0	1, 1, 1	0, 0, 0		0, 0, 0	0, 0, 0	1.00	1
Ease of process	0, 0, 0	0, 0, 0	1, 1, 1	1, 0, 0	1, 1, 1		1, 0, 0	2.67	2
High throughput	0, 1, 0	0, 1, 1	1, 1, 1	1, 1, 1	1, 1, 1	0, 1, 1		4.67	3

The team conducted a similar analysis to compare specifications of the hydrogel selection, shown in Table B. Based on the responses of the client, the team found that the range of elastic modulus is the most important, followed by range of stretch and biodegradable capabilities, then ease of preparation, ability to adhere to wells, and low cost.

Table B: Hydrogel Specifications Pairwise Comparison

	Range of Stretch	Range of Modulus	Remodelable/ biodegradable	Adheres to wells*	Ease of preparation	Low Cost	Total	
Range of Stretch		0, 0, 0	1, 0, 1	1, 0, 1	1, 0, 1	1, 1, 1	3.00	3
Range of Elastic Modulus	1, 1, 1		1, 1, 1	1, 1, 1	1, 1, 1	1, 1, 1	5.67	4
Remodelable / biodegradable	0, 1, 0	0, 0, 0		0, 1, 1	1, 1, 1	1, 1, 1	3.00	3

Adheres to wells*	0, 1, 0	0, 0, 0	1, 0, 0		0, 0, 0	0, 1, 0	1.00	1
Ease of preparation	0, 1, 0	0, 0, 0	0, 0, 0	1, 1, 1		1, 1, 1	2.33	2
Low Cost	0, 0, 0	0, 0, 0	0, 0, 0	1, 0, 1	0, 0, 0		0.67	0

Appendix D: Aggregate Creation Protocol

Materials

- Agarose powder
    - (Gelling temp 1.5%, 34.5-37.5°C; Gel Strength 1%: >1,200 g/cm^2)
- DPBS (-)
- PDMS molds, Sigma Aldrich
    - 1 400μL wells
    - 1 300μL wells
- Standard culture media
- Valvular interstitial cells (VICs)

Procedure

1. Autoclave necessary tools for making the aggregates such as forceps and razor blades.
2. Microwave Agarose bottle with cap slightly loosened in 10 second intervals until it is completely a liquid.
3. In the culture hood, pipette 400μL of agarose into a mold trying to reduce bubble formation and ensure the top of the mold is flat so it will sit nicely in the culture dish.
4. Allow to cool for ~10 minutes then push them out into 35mm culture dishes.
5. Add a small amount of media around the mold to prevent shriveling.
6. Repeat this until there are a total of 2 molds, 1 having well diameter 400μL and 1 having well diameter of 300μL.
7. Pipette 1e6 VICs in at least 100μL into each agarose mold trying to evenly distribute the cells while pipetting, then fill up the remaining room in the mold with culture media. In two of the molds add standard culture media supplemented with 250 μM AA.
8. Allow to sit in the incubator for 5 minutes to allow cells to fall into wells.
9. Remove from the incubator and add culture medium surrounding the mold until it is just about level with the top.

Appendix E: Collagen Protocol

Purpose
To create a 1 mL quantity of collagen gel

Materials

- 5X DMEM Supplemented with 10% FBS and 1% AA
- 0.1N NaOH
- Collagen - Corning, 4.07 mg/mL, Rat Tail Type 1 in 0.02 N acetic acid

Procedure

1. Complete the entirety of the experiment over ice.
2. Add 500 µL collagen (Corning, 4.07 mg/mL, Rat Tail Type I in 0.02 N acetic acid) to an Eppendorf microcentrifuge tube.
3. Add 500 µL 5X DMEM. Mix by pipetting up and down. The solution should be yellow or yellowish orange. Note the color.
4. If the color is too light, add 5 µL increments of NaOH as necessary until in the appropriate range.
5. Transfer mixture to a small labelled dish for the solution to polymerize.
6. Set in incubator at 37°C for one hour.
7. Observe consistency and any size changes.

Appendix F: Fibrin Protocol

Protocol obtained from personal notes of Ying Lei

Purpose
To create fibrin gels

Materials

- 0.9% NaCl
- 40 mM $CaCl_2$
- DI water
- Fibrinogen
- Thrombin
- DPBS

Procedure

Making fibrinogen stock solution

1. Make 0.9% NaCl solution by dissolving 360 mg NaCl in 40mL DI water
2. Agitate until dissolved and warm up to 37°C
3. Dissolve fibrinogen powder in NaCl to 16.7 mg/mL
4. Gently agitate for at least 30 minutes
    a. Do NOT vortex
    b. Can be left overnight at 37°C
5. Filter (0.2 μm) using syringe
    a. Not vacuum
6. To store, keep frozen at -20°C

Making thrombin stock solution

1. Dissolve thrombin lyophilized powder in $CaCl_2$ to 25 units per mL
    a. Use a syringe to add $CaCl_2$ to thrombin in vial
2. Agitate to mix completely
3. To store, keep frozen at -80°C

Making hydrogel

1. Thaw fibrinogen and thrombin stock solutions
    a. Fibrinogen can be thawed in a water bath if non-sterile
    b. Thrombin will thaw with handling alone as it is extremely sensitive to temperature
2. Dilute fibrinogen stock solution to 6.68 mg/mL using DPBS
3. Dilute thrombin to 2 units per mL using DPBS

4. Mix fibrinogen and thrombin 1:1 by pipetting gently and incubate about 30 minutes to overnight at 37°C

Observations from Ying: Fibrin gels might be too soft for the purpose of this experiment, it allows for cell migration. Migration can be reduced by adding Hyaluronic Acid (HA) which can help with the stiffening of the fibrin gel.

Appendix G: GelMA+HAMA Protocol

Purpose

To create a 1 mL quantity of GelMA+HAMA co-gel

Materials

- GelMA
- HAMA
- Igracure
- DPBS

Procedure

1. Add 5% wv GelMA (0.07 g) to a glass vial.
2. Add 1% wv HAMA (0.014 g) to the same vial, along with 0.5% wv Igracure (0.007 g).
3. Add 1mL DPBS to the same vial.
4. Place the vial in a water bath and heat until melted fully.
5. After pipetting the gel into the appropriate wells, cure it under a UV light for 30-90 seconds.

Appendix H: CellScale Settings

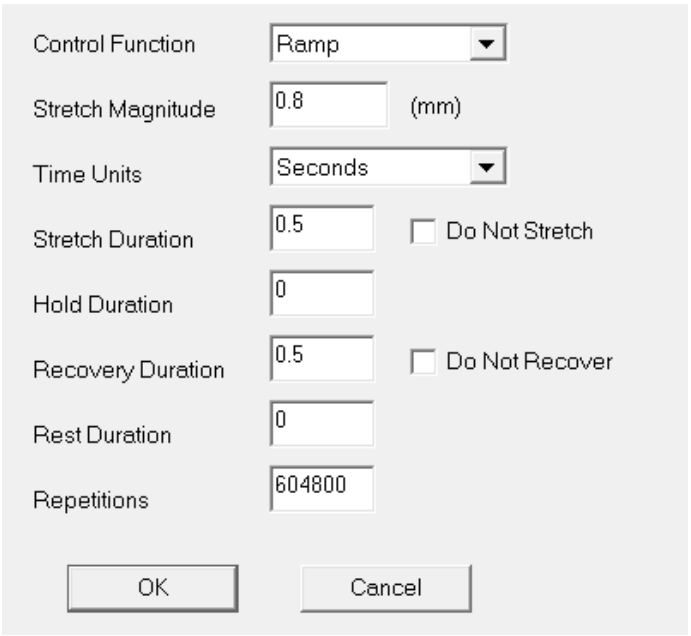

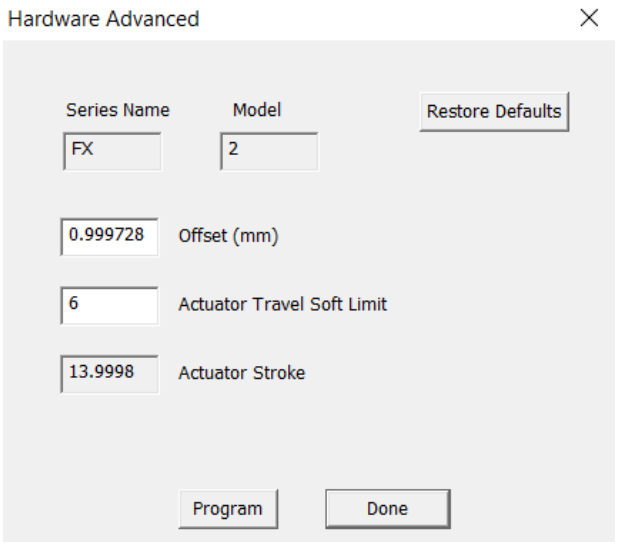

Appendix I: Live/Dead Staining (Propidium Iodide and Calcien)

Purpose

To live/dead stain 1mL of the 3D construct

Materials

- DPBS
- 4mM calcien
- 10 1mg/mL propidium iodide

Procedure

1. Combine 1mL DPBS, 0.5 µL calcien, and 10 µL propidium iodide, limiting light exposure since they are light sensitive.
2. Aspirate media from hydrogels.
3. Add the quantity of staining solution equal to that used to hydrate the gels.
4. Incubate for 30 minutes.
5. Image with a fluorescent microscope: calcien on a green channel and propidum iodide on red.

Appendix J: Von Kossa Calcification Staining

Purpose

To stain the 3D construct for calcification

Materials

- 1% Aqueous Silver Nitrate Solution
- 5% Sodium Thiosulfate
- 0.1% Nuclear Fast Red Solution

Procedure

1. Aspirate media from constructs.
2. Add 1% silver nitrate solution to fill wellplate.
3. Incubate under ultraviolet light for 20 minutes.
4. Rinse in several changes of distilled water.
5. Fill well with 5% sodium thiosulfate. Let sit for 5 minutes.
6. Rinse with several changes of distilled water.
7. Add volume of nuclear fast red solution equal to that used to hydrate. Let sit for 5 minutes.
8. Rinse in distilled water.
9. Image under brightfield for calcification (deposits will be dark, nuclei will be red).

Appendix K: Matlab data

The code in Matlab to plot the smooth contour map is below:

[C,h] = contourf(X,100);set(h,'LineColor','none');

Where "X" is a matrix of strain data.

When the data is initially extracted from PIV lab, it is in terms of strain rate. This strain rate needs to be multiplied by the time increment between each frame, which is ~ 0.03 seconds. There are 16 data points in each frame. Each corresponding data point is added together from each frame to give the final strain distribution map. Below is the added strains for each data point in the Y direction. The second image is for the X direction.

4.12250821	2.147359715	3.282409208	3.377986765	2.19105608	2.251419119	1.65046203	1.32033662
2.05772275	2.34363034	2.09891087	1.88448843	1.65887787	1.878158397	1.712904273	1.214181506
10.361386	9.704290332	6.995379468	4.012541214	5.90528047	5.56745869	5.65016496	7.219141842
7.77524745	9.457095615	6.007392679	5.545874532	8.42904282	8.575907505	7.131023031	7.430692995
8.54191411	8.776567569	10.08745865	10.82145204	11.7171616	10.20891079	8.551485063	7.310659993
9.82838274	10.83498339	12.28151803	13.32343221	12.4376236	11.46237612	9.500990004	7.51485141
6.98382831	9.213201228	10.19966987	10.23762366	9.40462037	9.451155021	8.621122026	6.542574192
7.93564349	9.540923997	8.988448755	8.61716163	8.57854777	8.092079127	8.066666586	7.391848111

0.02748339	0.014315731	0.021882728	0.022519912	0.01460704	0.015009461	0.01100308	0.008802244
0.01371815	0.015624202	0.013992739	0.012563256	0.01105919	0.012521056	0.011419362	0.008094543
0.00690759	0.006469527	0.004663586	0.002675027	0.00393685	0.003711639	0.003766777	0.004812761
0.0051835	0.00630473	0.004004928	0.00369725	0.00561936	0.005717272	0.004754015	0.004953795
0.00569461	0.005851045	0.006724972	0.007214301	0.00781144	0.006805941	0.00570099	0.004873773
0.00655226	0.007223322	0.008187679	0.008882288	0.00829175	0.007641584	0.006333993	0.005009901
0.00465589	0.006142134	0.00679978	0.006825082	0.00626975	0.00630077	0.005747415	0.004361716
0.00529043	0.006360616	0.005992299	0.005744774	0.00571903	0.005394719	0.005377778	0.004927899

The following images show the displacement and strain % at frame 1, 5, 10, and 14 (max stretch). Frame 14 was chosen instead of 15 because this is when there is the maximum stretch, frame 15 is when the device pauses before continuing back to its original position.

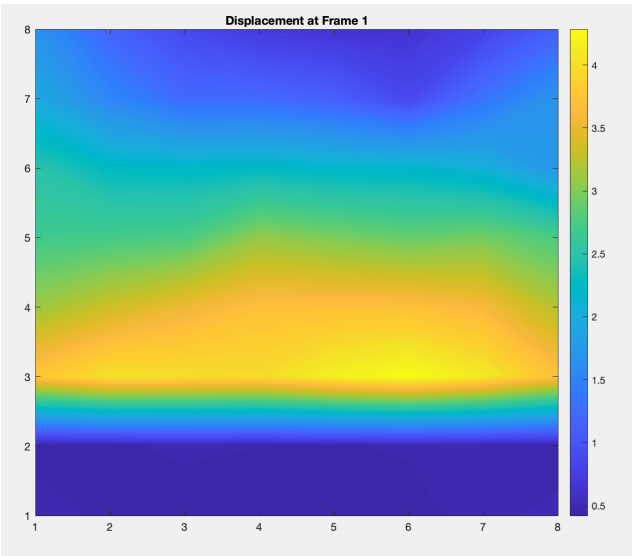

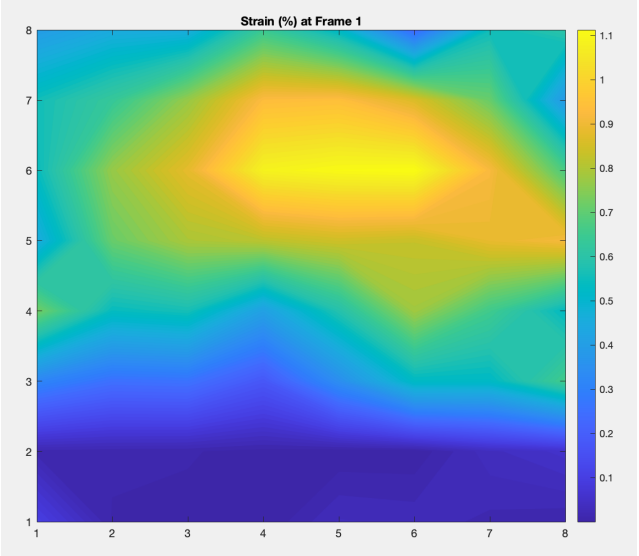

Frame 1

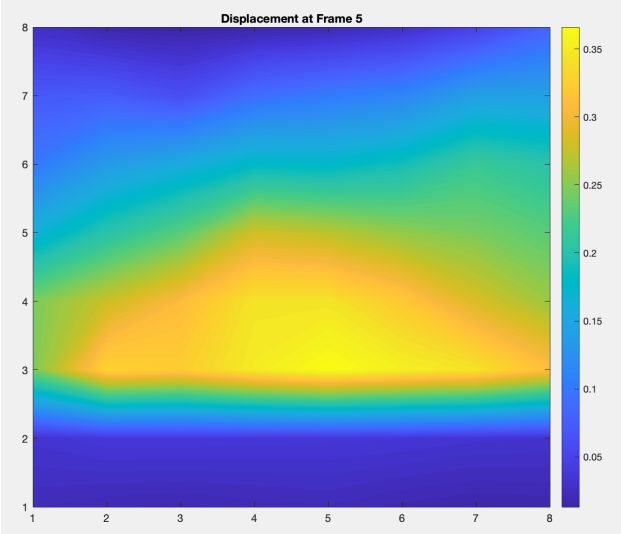

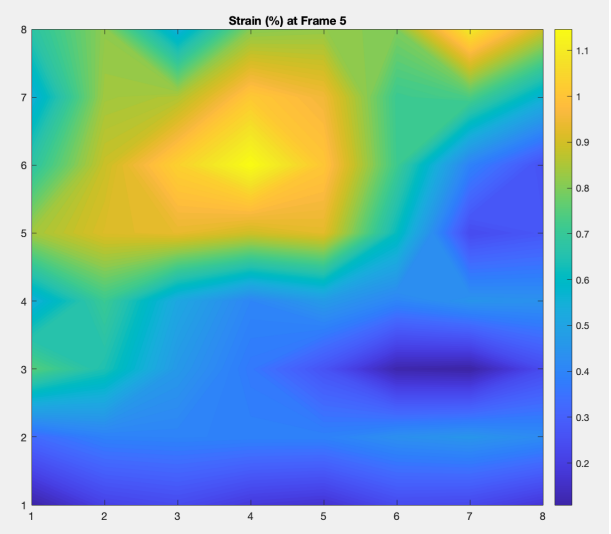

Frame 5

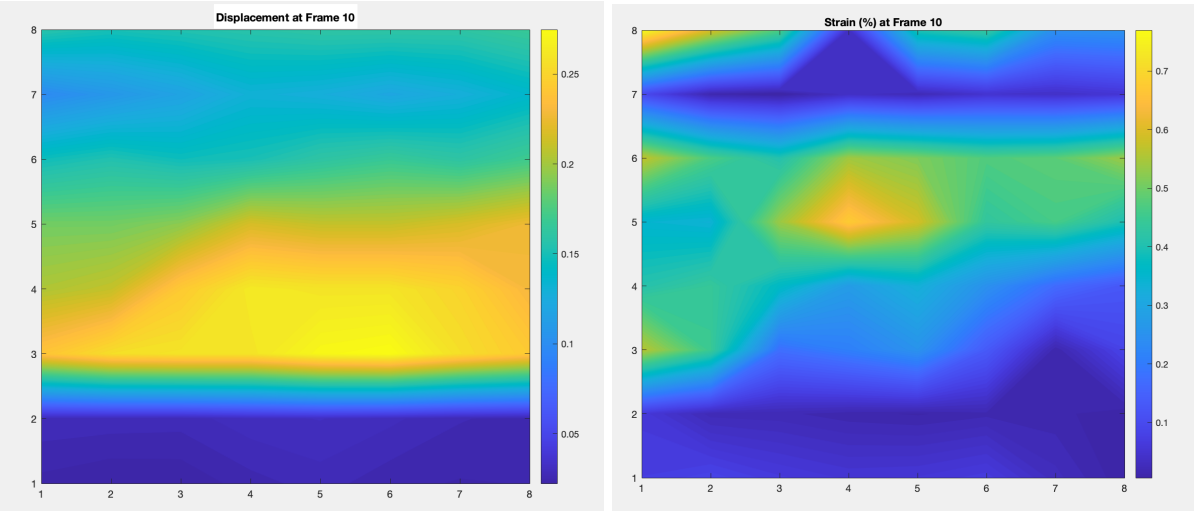

Frame 10

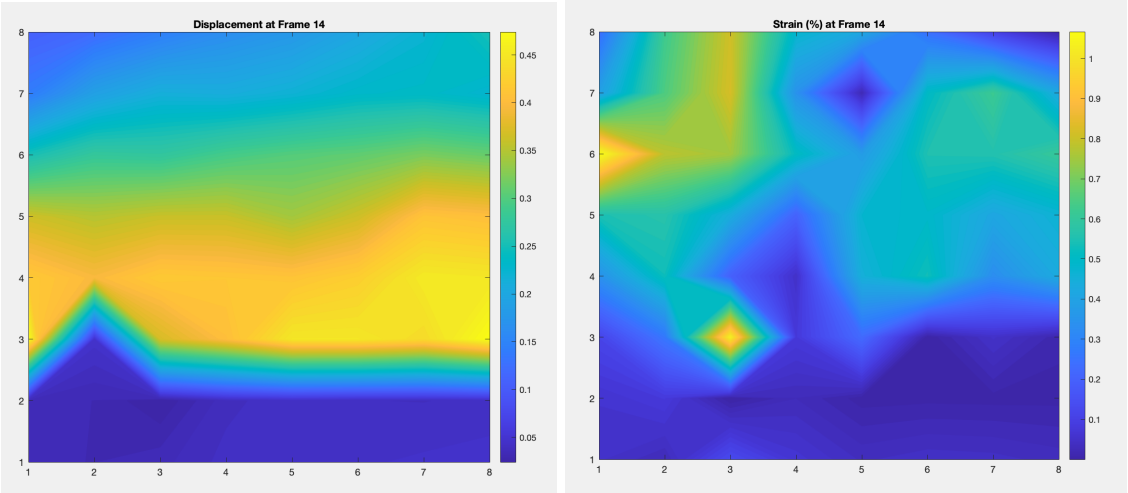

Frame 14

The images below show the progression of strain as each frame is added. The first image is strain at frame 1, then added strain for frames 1-5, then added strain for frames 1-10, then added strain for all 15 frames.

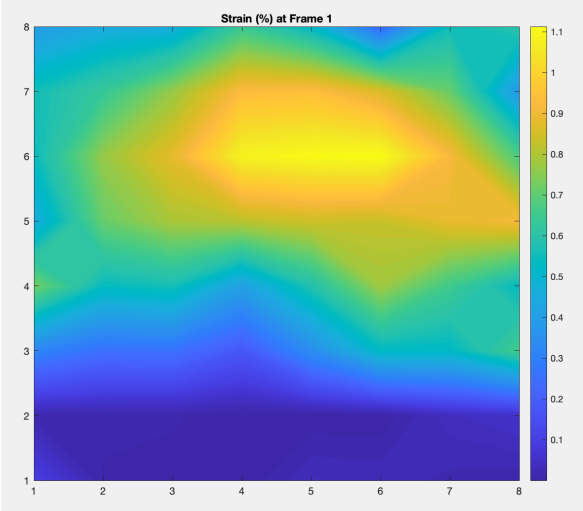
Strain (%) at Frame 1
8
7
6
5
4
3
2
1
1 2 3 4 5 6 7 8
1.1
1
0.9
0.8
0.7
0.6
0.5
0.4
0.3
0.2
0.1

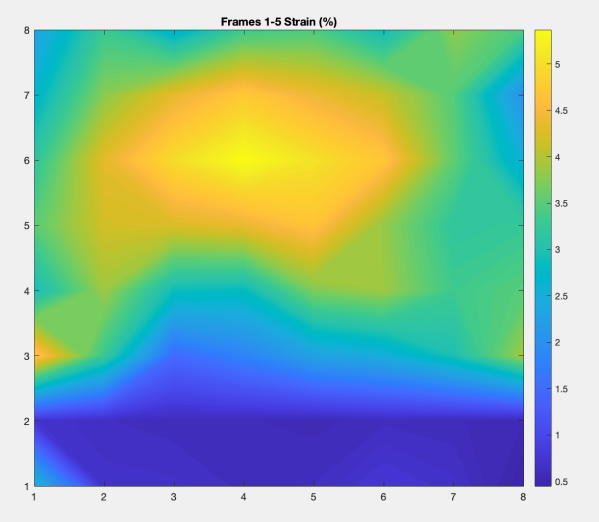
Frames 1-5 Strain (%)
8
7
6
5
4
3
2
1
1 2 3 4 5 6 7 8
5
4.5
4
3.5
3
2.5
2
1.5
1
0.5

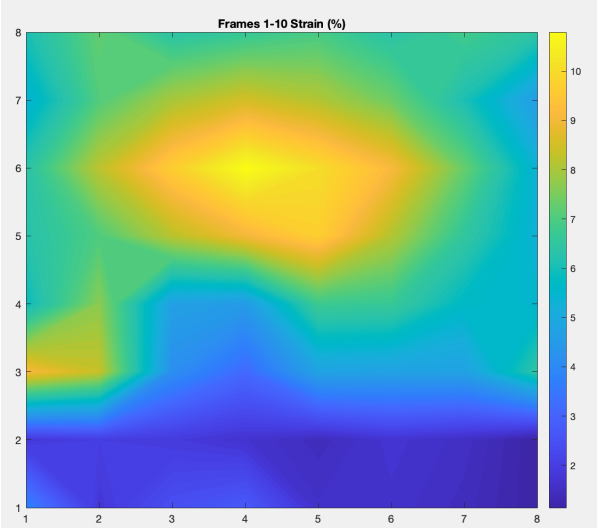
Frames 1-10 Strain (%)
8
7
6
5
4
3
2
1
1 2 3 4 5 6 7 8
10
9
8
7
6
5
4
3
2

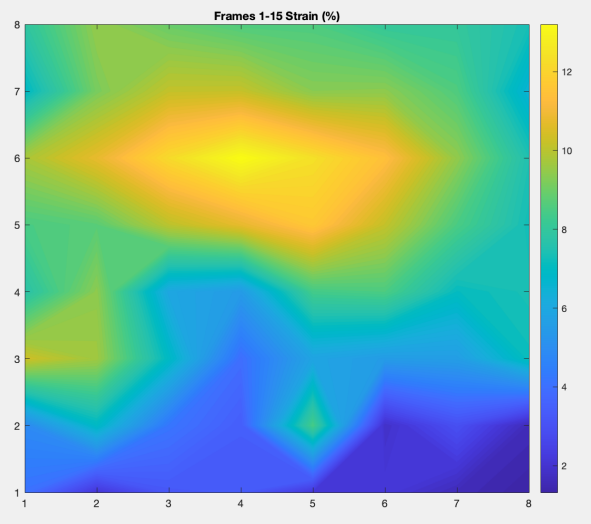
Frames 1-15 Strain (%)
8
7
6
5
4
3
2
1
1 2 3 4 5 6 7 8
12
10
8
6
4
2